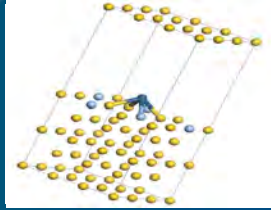
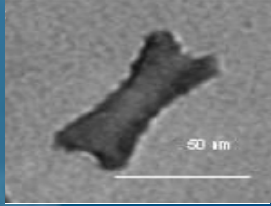
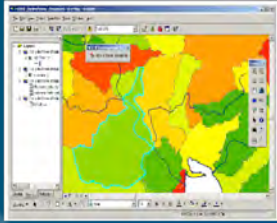


# SRNL LDRD Annual Report 2010



# From the Laboratory Director



I am pleased to have the opportunity to introduce the 2010 Laboratory Directed Research and Development (LDRD) Annual Report. This important program displays both the breadth of SRNL's research efforts and the depth of our commitment to expand the capability and mission impact of this Laboratory. We continue to broaden participation in the LDRD program across the Laboratory while maintaining our record of innovative technical accomplishment.

We are now starting to see some very exciting results from the initial Strategic Initiatives that were funded at the end of FY09. David Hobbs, working with team members from SRNL, the University of Washington, and Sandia, has shown that the nano-scale titanate materials they have developed actually inhibit growth of some types of cancer cells and have anti-bacterial activity as well. Ted Motyka and co-workers are developing high capacity portable power sources based on SRNL's alane chemistry. David Werth is proving the value of some very innovative approaches in identifying the

impacts of climate change on future energy production. Ming Au is making great strides in developing rechargeable lithium-air and lithium-ion batteries with higher capacity and greater safety, at lower cost than current lithium batteries.

We are also seeing projects aligned with SRNL's primary business areas make new and exciting advances of potential value to our customers. In the Nuclear and Homeland Security arena, Ken Gibbs and co-workers in EES have demonstrated the feasibility of using video cameras as radiation detectors. This could have an immediate impact on our plant customers as well as providing a new tool to aid in the cleanup after a dirty bomb. To cope with the impending shortage of He-3, Steve Serkiz and his "nano-team" have demonstrated the feasibility of boron-based materials as neutron detectors.

As DOE-EM's National Laboratory we continue to expand the tools available to pay down the legacy of wastes from the Cold War. Mark Williamson demonstrated a new and more robust method for evaluating the suitability of metal alloys as waste forms for certain types of waste. Anna Knox and Ken Dixon completed their work on the use of amendments for enhanced soil remediation by demonstrating their long-term performance.

In addition to the energy-related projects that will enhance our nation's Energy Security already mentioned, the work of Steve Sherman and co-workers on lignin must be spotlighted. Steve and his team have demonstrated the feasibility of a biological route to breaking down lignins for conversion to bio-fuels and other chemicals. This will greatly increase the potential for using cellulosics as a source for bio-fuels.

The scientific and engineering progress described in this Annual Report will provide the foundations for future programs that will help SRNL maintain its position as DOE's premier applied science and engineering laboratory. SRNL's researchers have again shown that the LDRD program is a sound investment by the Laboratory that will pay dividends to both the Laboratory and the nation in the future.

A handwritten signature in black ink, appearing to read "Terry Michalske". The signature is fluid and cursive, with a long horizontal stroke at the end.

Dr. Terry Michalske



## Table of Contents

From the Laboratory Director.....	i
Table of Contents.....	ii

### Project Summaries, *Principal Investigator*

<b>Nanosize Titanates for Optimized Performance in Separations Science, Innovative Medical Applications and Photochemistry, <i>D. T. Hobbs</i></b> .....	1
<b>Video Image-Based Radiation Detection and Measurement, <i>K. N. Gibbs</i></b> .....	3
<b>Bio-Decomposition of Lignin for Production of Liquid Fuels, <i>S. R. Sherman</i></b> .....	4
<b>Development of High Capacity Portable Power Systems, <i>T. Motyka</i></b> .....	6
<b>Solid Polymer Electrolyte for Mg-Ni Rechargeable Batteries, <i>B. Garcia-Diaz</i></b> .....	8
<b>Self Assembly of Shape-Selective Catalyst Impregnated Membranes: Towards Direct Methanol Fuel Cells (DMFCs), <i>S. E. Hunyadi-Murph</i></b> .....	11
<b>Advanced Batteries for Electric Energy Storage, <i>Ming Au</i></b> .....	13
<b>Thermodynamic evaluation of metallic waste forms, <i>Mark Williamson</i></b> .....	15
<b>Sorption of CO<sub>2</sub> into Supported Ionogels for Advanced Carbon Sequestration Technologies, <i>J. Gray</i></b> .....	17
<b>Structure Property Relations in Mixed Ionic/Electronic Conductive Ceramics for Energy Conversion, <i>K. S. Brinkman</i></b> .....	20
<b>The Impact of Climate Change on Future Energy Production in the Southeast US, <i>David Werth</i></b> .....	23
<b>Fast Neutron Irradiation of Advanced Ceramics for Extreme Environments, <i>E.N. Hoffman</i></b> .....	25
<b>Organo-Boron Chemistries: Probing Variations in Lewis Acidity of Substituted Boroxines, <i>L. C. Teague</i></b> .....	27
<b>Formation of Actinide Solid-Solution Oxides by Co-Precipitation of Actinide Oxalates, <i>G. F. Kessinger</i></b> .....	29
<b>Nanoscale Boron Based Neutron Detectors, <i>Steven Serkiz</i></b> .....	31
<b>Evaluation of the long-term effectiveness of enhanced soil remediation with mixed amendments using geochemical parameters under field conditions, <i>A. S. Knox, K. L. Dixon</i></b> .....	34
<b>Advanced Gas Sensors Using SERS-Activated Waveguides, <i>R.J. Lascola</i></b> .....	35
<b>Nano-Composite Hybrid Lithium-Ion Battery, <i>H. R. Colón-Mercado</i></b> .....	38

# 2010 Laboratory-Directed Research and Development Program Annual Report

## Project Summaries

### **Nanosize Titanates for Optimized Performance in Separations Science, Innovative Medical Applications and Photochemistry**

*D. T. Hobbs; M. C. Elvington, K. M. L. Taylor-Pashow, J. Wataha (U. Washington),  
M. D. Nyman (SNL)*

*SRNL has been using titanate-based materials to effect separations in waste solutions for several years. This Strategic Initiative is targeting development of nano-sized titanates for use in separations, medical applications and photochemistry. Progress has been made in synthesizing nano-sized titanates and peroxotitanates. Somewhat surprisingly, several of the titanates have been shown to inhibit growth of cancer cells, and to have anti-bacterial properties. Enhanced photocatalytic activity for one of the materials has been demonstrated. Testing of the separations capabilities of these materials is underway.*

Titanate materials are remarkably effective ion-exchange materials for the decontamination of radioactive and industrial wastewater solutions. Recently, these materials have been shown to be effective for the delivery of biologically relevant metals to living cells under physiological conditions. This earlier work used fine powders that are about 1 to 10 microns in size. This project seeks to synthesize titanate materials that feature nano-scale particle sizes. We believe that nanosize titanates will offer superior performance in chemical/radiochemical separations and innovative medical applications. Furthermore, modification of the nanosize titanates could provide photoelectronic properties that could be exploited for new applications in photocatalysis and photovoltaics.

Good progress has been made on the synthesis of nanosize titanates and peroxotitanates using three different synthetic strategies. In the first strategy, micron-sized sodium or cesium titanates are delaminated by treating with tetrabutylammonium (TBA) hydroxide. TEM images indicate these materials have thin fibrous and sheet-like particle morphology with thickness well below 20 nm.

In the second strategy, nanosize titanates are produced by modifying the sol-gel process used to prepare micron-size sodium titanates. Process modifications include reagent dilution, method of reagent addition and presence of surfactants. The combined modifications produce materials with sizes ranging as low as 25 nm in size as measured by a dynamic light scattering technique.

The third strategy produces sodium titanate nanotubes by heating a mixture of titanium

dioxide and concentrated sodium hydroxide in a sealed reactor at 110 C for 24 hours, which produces tubular nanosize sodium titanates.

The corresponding peroxotitanates of each of the nanosize titanates are produced by treating the titanates with hydrogen peroxide. Currently we are drafting a publication detailing the synthesis and characterization of the nanotitanates. The sol-gel synthesis method may be sufficiently novel to warrant filing for a patent.

Testing of the titanates during FY10 focused on the following three areas. Do the metal-exchanged forms of the titanates inhibit the growth of cancer cells and bacteria? Do the peroxotitanates offer improved photocatalytic properties? Do the nanosize titanates offer improved performance for the removal of metals ions from waste solutions?

The oxidation (i.e., decomposition) of methyl orange is serving as an indicator of the photocatalytic activity of the nanosize titanates and peroxotitanates. In this reaction, the methyl orange (MO) is dissolved and irradiated with UV light in the presence of catalyst. For this evaluation we selected a commercially available titanium dioxide powder (Degussa P25), from which we isolated a nanosize fraction. The peroxotitanate sample prepared from the cesium titanate precursor exhibited slightly better MO oxidation performance than the other research samples (not shown in figure) and clearly better when compared to the nanosize fraction of the Degussa material. Thus, the nanosize materials produced by the delamination synthesis appear to have promise as photocatalysts. Studies are in progress testing the photocatalytic characteristics of the nanotitanates prepared by the other synthetic strategies.

Testing at the University of Washington has shown that several metal-exchanged forms of micron-size titanates inhibit various oral-based cancer cells. Testing indicates that the addition of the titanate materials in dental composite formulations has shown excellent mechanical strength. Furthermore the metal-exchanged titanates and peroxotitanates also suppressed the growth of oral-based bacteria cell lines. This finding was quite unexpected with the micron-size materials since it was felt that the micron-size materials would be too large to successfully interact with the bacteria.

Testing recently initiated evaluating the ion-exchange characteristics of the nanotitanates prepared by all three synthetic methods. Metal-ion exchange testing featured measuring the removal of strontium and actinides (Pu, Np and U) from high-level waste solution and the removal of metal ions (e.g., Au, Pt, Pd) from aqueous solutions. Results with the nanotitanate and peroxotitanates produced by the delaminated method exhibited similar performance compared to micron-sized titanates for the separation of Sr and actinides from an alkaline salt solution. Analyses are in progress to determine the Sr and actinide-removal performance of the nanotitanates and peroxotitanates prepared by the sol-gel and hydrothermal methods.

Testing indicated that the sol-gel and hydrothermal-prepared nanotitanates exchange

Au(III) ions from both aqueous and buffered saline solutions. The sol-gel nanotitanates exhibited much higher affinity for Au(III) than the hydrothermal nanotitanates as well as the micron-sized titanates. Additional tests with other metal ions are in progress.

### **Video Image-Based Radiation Detection and Measurement**

*K. N. Gibbs; Monica Phillips, Melissa Sindelar, Rebecca Barrier*

*Video cameras have become ubiquitous devices in our everyday lives. It is well-known that when exposed to radiation, the video image degrades due to speckling. The goal of this project was to determine whether this effect could be quantified thus enabling video cameras to act as radiation detectors as well. Feasibility was demonstrated. It appears that the technique may be applicable to radiation exposures of 3 mR/hr. If results continue to be positive, thousands of video cameras already in use by government agencies, commercial entities, and law enforcement could be used to monitor for the introduction of radiation sources near the cameras. Additionally, remote viewing cameras deployed in DOE facilities could obtain radiation dose rate information while performing visual inspections as an added feature.*

Video cameras used for remote inspections at SRS have demonstrated a visible speckle effect (i.e. white spots) in the video image when in the presence of a radiation field. This effect is caused by direct interaction of high energy photons with the camera chip. This interaction creates a large number of electron-holes pairs in a localized region nominally the size of a single pixel. This may result in that pixel becoming saturated (i.e., maximum intensity or maximum charge collection capacity). The number of pixels affected appears to be proportional to the radiation exposure or dose rate. Furthermore, if the pixel is not saturated, the amount of charge (or equivalently the digitized value) may provide information regarding the energy of the interacting photon.

The goals of this research were to determine the feasibility of using a video camera to detect radiation and provide radiation exposure or dose rate information. The goal is not to replace conventional radiation detectors with a video image-based system but to take advantage of the video camera's response to radiation for dual purpose usage. Specifically, in situations where cameras are pre-existing, they could be used for radiation detection as well as their primary intended application.

The data was collected over radiation exposure levels ranging from 250 mR/hr up to 7000 R/hr. The lower range sensitivity could easily be on the order of 3 mR/hr or perhaps lower. In most cases, the radiation response was found to be linear with exposure rates. The B&W cameras showed significant camera-to-camera variation, thus each camera should be calibrated with its own threshold setting to optimize performance. The color CCD cameras did not exhibit the camera-to-camera variation and may offer the ability for a generic calibration and threshold selection. This would have obvious benefits for situations where there are a large number of cameras to be used and where individual

calibration would be too costly or time consuming. However, more than two cameras of a particular design would need to be tested before that conclusion could be properly made.

It has been shown that several factors influence the cameras response such as threshold setting, automatic electronic features, lens settings, and lighting condition to name a few. These factors will need to be controlled or a method to correct for changes in these factors will be needed. It was also determined that the response is highly variable from frame-to-frame and multiple images (~1000 frames) are needed for accuracy. It appears that there may be an angular dependence, but there were conflicting results between the B&W and color camera results. Further testing is needed in this area. No correlation between speck intensity and photon energy was found. Therefore, the speck intensity will not be useful for energy discrimination as was expected. No work was performed regarding operational lifetime and degradation of performance over time. There was no degradation noted on any of the cameras over the period of testing even though the exposure rates were as high as 7000 R/hr.

The results of this research could immediately applicable at SRS. For example, all canyons have numerous cameras installed on the overhead cranes. Without installing any new equipment, this new method could be used to continuously monitor radiation levels within the canyon as the crane is moved. As a second example, all video cameras used to perform routine remote visual inspections could also provide radiation field information without having to install radiation detectors, additional wiring, or other hardware.

### **Bio-Decomposition of Lignin for Production of Liquid Fuels**

*S.R. Sherman; C.E. Turick, T.J. French Sr., J.M. Henson (Clemson University)*

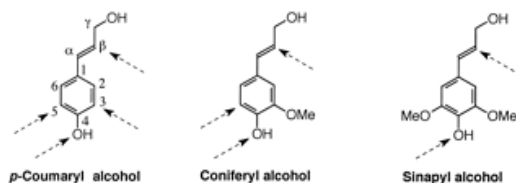
*In fermentation-based cellulosic biofuels production facilities, lignin is separated from biomass feedstocks as an inert side product. In this work, a controllable biological method for breaking down lignin into its constituent fragments and monomer units was sought for the purposes of allowing lignin to be more easily fashioned into biofuels and other chemicals. Certain micro-organisms metabolize lignin, and it is the purpose of this project to mimic their methods to accomplish the partial degradation of lignin into its constituent monomers. Although this task may be accomplished using high-temperature chemical processing (i.e., pyrolysis), a biological method would likely be more energy efficient and would not require the use of more expensive heat-resistant materials. This project identified suitable organisms, and demonstrated process feasibility.*

The U.S. Department of Energy is targeting the production of biofuels from cellulosic feedstocks as the next area for expansion in its efforts to find substitutes for petroleum-based fuels. The category of cellulosic feedstocks includes corn stover, grasses, wood, and any other non-food plant material containing cellulose, which can be broken down into sugars and fermented or gasified to make liquid fuels.

Most terrestrial plants, including grasses and trees, contain between 20-40% lignin. Lignin, due to its highly polymerized cross-linked structure, is chemically inert to the enzymes and organisms used to ferment sugars into fuels, and so becomes a low-value waste material in such processes. If lignin could be decomposed into its constituents (see figure for constituent type), then it would be much more chemically active and amenable to the manufacture of liquid fuels.

In nature, organisms such as white rot fungi and microorganisms in the gut of termites metabolize lignin as a food source. Unfortunately, these organisms cannot be used directly in a fermentation-like process to degrade lignin, because there is yet no known method to get them to stop metabolizing the lignin once it is decomposed into fragments of the desired size and type, and the organisms will continue to digest the fragments until only CO<sub>2</sub> and other metabolic waste products remain.

This project aimed to take advantage of the free radical chemistry that governs lignin breakdown in natural organisms. Development of suitable analytical techniques is thus of crucial importance. Ultimately, control of the degradation process is sought so that the decomposition of lignin into fragments that are useful for liquid fuels production can be performed in a reliable and predictable manner.



Principle Lignin Monomers

Partial degradation of lignin was pursued by generating reactive oxygen species in a surrounding aqueous phase containing microbial species. The reactive oxygen species include: hydroxyl radicals formed by Fenton-like reactions of Fe(III) to Fe(II) coupled with bacterial H<sub>2</sub>O<sub>2</sub> production, and by the reduction reactions of nitrous oxide, N<sub>2</sub>O, to nitrogen, N<sub>2</sub>, as performed by denitrifying bacteria. Control of free radical formation is performed by controlling the flow of reactants into the test cells, and the growth conditions of the bacteria species that are generating the hydroxyl radicals. The goal is to decompose solid lignin to a liquid or a multi-phase liquid mixture at room temperature that is amenable to commercial crude oil refining techniques.

Experiments using species from the genus *Shewanella* (*oneidensis* and others) were performed to test the iron reduction reaction mechanism, and the species *Paracoccus denitrificans* and *Pseudomonas denitrificans* were used to perform the nitrogen reduction mechanism. These organisms do not use lignin as a food source, but they do have the ability to generate the desired hydroxyl radicals which are needed to attack lignin's chemical bonds.

Initiation of lignin degradation in the case of *Shewanella* was induced by changing the test cell atmospheric conditions from anaerobic to aerobic, which induces Fe(II) accumulated in the test environment after a certain period of growth to drive the formation of hydroxyl radicals. Initiation of lignin degradation in the case of the denitrifying bacteria species was induced by introducing a flow of N<sub>2</sub>O to the test cells.

Results from these experiments indicate that degradation of lignin into fragments is possible using both degradation mechanisms, and chemical analyses of samples reveal an increase in the diversity and amount of lignin degradation compounds in the broth with increasing exposure time.

These results are qualitative in nature, and no information is yet available to quantify how quickly the degradation process may be carried out, and to what extent this degradation process may be carried out before bacterial metabolic actions become inhibited by the build-up of degradation products in solution. More experiments are needed at longer exposure times to allow lignin degradation products accumulate in the liquid phase to the point where 1) bacterial cell growth and functioning is stopped due to the inhibitory effects of the degradation productions or 2) the liquid phase becomes saturated with lignin degradation products and forms a second liquid phase without stopping the degradation reactions.

Future work on this topic will be carried out under an existing SRNL-Clemson University collaboration that is focused on developing the technologies to enable the efficient production of biofuels such as ethanol or butanol from switchgrass, sorghum, and trees such as yellow pine and sweet gum.

### **Development of High Capacity Portable Power Systems**

*Theodore Motyka; Ragaiy Zidan, Kit Heung, Joseph Teprovlch, Douglas Knight, Long Dinh*

*The goal of this Strategic Initiative is to develop high capacity portable power systems based on advanced hydrogen storage materials coupled with small fuel cells and other hybrid technologies. Significant progress has been made toward achieving this goal, including development of a new and potentially lower cost process for producing alane, reducing the volume of alane, and increasing the amount of hydrogen released through addition of another metal hydride.*

The specific energy densities of state-of the-art batteries vary from 150 Wh/kg for secondary Li batteries to less than 400 Wh/kg for primary Li batteries. The DoD and commercial portable equipment manufacturers are requesting specific energy densities greater than 1000 Wh/kg – more than 2 to 3 times that of the best primary Li batteries today. Hydrogen with the highest energy density of any fuel at 33,000 Wh/kg (more than twice that of gasoline) has the greatest potential to meet this goal. Even when coupled

with a fuel cell at 50% efficiency and a hydrogen storage material with 10 wt % hydrogen, a power system with > 1,000 wh/kg is doable.

DOE has invested numerous years and millions of dollars to develop advanced hydrogen storage materials for automotive applications. Many of these materials have demonstrated very high hydrogen capacities (greater than 20 wt%) but many do not meet all the many requirement needed for automotive applications. Many of these materials, however, may very well be viable on small portable systems. The goal of this research is to develop small power systems (2-3 X better than today's best battery technology) around novel advanced hydrogen storage materials coupled with small fuel cells and other hybrid technologies.

SRNL as part of the DOE Center of Excellence in Metal Hydrides has been working on developing several light-weight, high capacity solid-state hydrogen storage materials. One of the most promising materials is aluminum hydride or alane. Aluminum Hydride (alane) is much safer to handle and process than many other high capacity complex hydrides that can be used in a fuel cell system. This material can store and deliver 10wt% hydrogen at temperatures less than 100° C, which is compatible with DOE's fuel cell requirements. In addition, the spent aluminum powder, following initial hydrogen desorption, can be reused to deliver additional hydrogen by reacting with water and alkaline hydroxide. The two reactions will result in delivering up to 20% hydrogen by weight to fuel devices in the field.

Alane, while not a new material, has only in the last few years been considered as a hydrogen storage material for fuel cell applications. SRNL researchers are among only a handful of researchers, worldwide, currently working with alane and beginning to unwrap its material and engineering properties. The specific objectives of this proposed project are: 1) to characterize and optimize alane into a novel new hydrogen storage material 2) to develop a small hydrogen storage vessel containing alane and to demonstrate hydrogen release and delivery rates suitable to power small existing military fuel cells, and 3) to provide sufficient data and interest to develop a larger DoD funded Portable Power Center initiative, that will include alane and other higher capacity hydrogen storage materials as well as other energy storage technologies.

At the present time only a limited amount of commercial alane is readily available. As part of this project a new supplier of alane was identified to provide sufficient quantities of alane needed to carryout this project. A laboratory scale system was also developed to produce small initial quantities of alane for experimental and optimization studies. During the course of this work a new and potentially lower cost process for producing alane was developed. The novel process avoids the use of ether and is able to produce very pure adduct and halide free alane. An invention disclosure was submitted and a provisional patent is being filed.

In a military application, water can be obtained on the battlefield for extracting more power from the portable system. Therefore, after depleting alane from hydrogen the active aluminum can be reacted with water to produce more hydrogen (10% more hydrogen). One of the problems has been that the reaction with water often forms a gelatinous hydroxide that coats the aluminum and limits the extent of reaction and the amount of hydrogen released. A series of tests were performed to evaluate the alane and spent aluminum in aqueous reactions both with and without additives to enhance the amount of hydrogen that can be released. We were able to achieve an additional 10wt% hydrogen release by the addition of another hydride material such as NaH. A patent application is being prepared.

Alane powder was successfully compacted to enhance its volumetric density and to improve its performance in portable energy applications. A density increase of over 3X is possible without adversely affecting the hydrogen release rate from the pressed material versus the powder.

A hydride vessel and test system was designed and fabricated to evaluate the hydrogen release rate for small fuel cell applications. Results showed that the system can scale very nicely to meet the required release rate for a small 100 W fuel cell system. An internal report is being issued. SRNL has procured a small Parr reactor, equipment and additional chemicals to produce larger quantities of alane material. The design and fabrication of a second prototype vessel to operate a 100 watt fuel cell has been completed.

### **Solid Polymer Electrolyte for Mg-Ni Rechargeable Batteries**

*B. Garcia-Diaz; Joshua Gray, Charles James, M. Au and M. Kane*

*Research has been performed on polyethylene oxide (PEO) and polyvinyl alcohol (PVA) polymers impregnated with KOH for use as solid electrolytes in battery applications. It was found that PEO could not be synthesized at low enough crystallinity to have good conductivity. However, PVA based membranes could be synthesized with conductivities approaching the goal of 0.1 S/cm by addition of a nanoclay to reduce the crystallinity. This opens the door to a battery with significantly improved specific energy capacity and safety in a lower cost package than current nickel metal hydride or lithium batteries.*

Currently, automakers use nickel-metal hydride (NiMH) rechargeable batteries to power hybrid electric vehicles (HEV) with 375 mAh/g theoretical capacity. The carbon-Li intercalation Li-ion rechargeable batteries offer 500 mAh/g theoretical capacity. However, recent massive recalls of Li-ion rechargeable batteries raise serious concerns regarding safety, particularly in powering HEVs. The weight, material cost and safety represent three major challenges for current HEV battery technology. This project aims to both increase the capacity and drastically improve the inherent safety of current batteries.

Magnesium-nickel hydride ( $\text{Mg}_2\text{NiH}_4$ ) as the electrode material has 500 mAh/g of theoretical capacity with few of the safety related issues associated with Li-ion batteries. Magnesium is also an abundant and low-cost metal. There is no fire hazard associated with Mg-Ni aqueous solution rechargeable batteries. Unfortunately, the high electrochemical capacity of Mg (or Mg alloys) decreases very quickly after a dozen charging-discharging cycles due to severe corrosion in the aqueous alkaline solution. Using a non-aqueous solid polymer electrolyte (SPE) membrane to replace the caustic alkaline solution would prevent Mg corrosion. This new type of battery, referred to as the SPE Mg-Ni rechargeable battery, would be superior to the current NiMH and Li-ion rechargeable batteries in terms of specific energy capacity, safety and material cost.

The success of the non-aqueous SPE Mg-Ni batteries relies on the development of a suitable polymer membrane with high proton (or hydroxide ion) conductivity. The conductivity of aqueous alkaline (e.g. KOH) solution is about 0.4 S/cm, but even mature proton exchange polymer electrolytes such as Nafion<sup>®</sup> 117 only have conductivities around 0.08 S/cm and also require hydration. The lower conductivity of SPEs limits the pulse power of batteries at large discharge currents. The goal of this project is to increase the conductivity of anion exchange polymer electrolytes to 0.1 S/cm or higher through the use of ionically conductive polymers without the use of water.

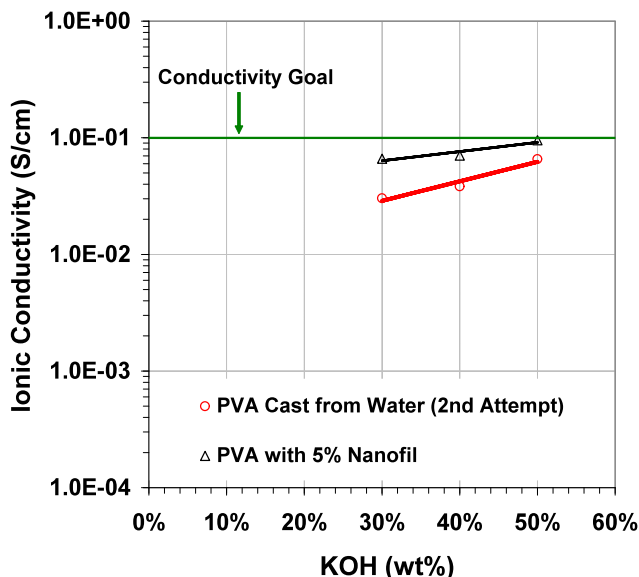
In Year 1 of this project the equipment necessary for electrolyte development was procured and the cycling of an Mg-Ni battery with a commercial solid polymer electrolyte was demonstrated. Examples demonstrating proof of principle for a patent application were also provided. During Year 1, it was also determined that a more alkaline salt in the polymer would produce higher ionic conductivity.

As a result, potassium hydroxide (KOH) was incorporated into the PEO. The conductivity of these electrolytes,  $\leq 10^{-3}$  S/cm, were improved, but still only on-par with literature results, but no major improvements were found. The lack of positive results in over 10 tests with the PEO combined with literature studies led to the testing of different polymers and polymer blends.

A more amorphous polymer, polyvinyl alcohol (PVA), was selected, based on literature results. The conductivity of the pure PVA polymer without KOH was near  $1\text{E-}6$  S/cm. When KOH was added to the PVA the conductivity greatly increased. The conductivity of electrolytes containing PVA with KOH (30 – 50 wt%) were on the order of  $10^{-2}$  S/cm. The samples show a strong dependence on KOH content, as expected, but also are significantly affected by synthesis procedure. Mixing time seemed to have the largest of synthesis parameters on the conductivity. Membranes cast after 3 hours of mixing appeared to have all the polymer dissolved and resulted in the best films. Too little mixing of the solution resulted in undissolved polymer, while longer mixing resulted in premature polymerization due to dehydration of the mixture.

Commercial polyelectrolytes (PADDAC and PDDAC) were procured and incorporated into PVA. The membranes synthesized with polyelectrolyte in PVA had conductivities near  $5E-4$  S/cm, but did not rise much above that value regardless of changes to the synthesis technique. This lower conductivity value with polyelectrolyte relative to membranes with KOH is most likely due to lower charge mobility and lower hydroxide concentration.

Adding a Nanofil clay to the polymer was also tested as a method to improve the hydroxide ion conductivity. Addition of 7% Nanofil caused a decrease in conductivity over the 30% KOH and PVA membrane. Similar results of higher conductivity with lower amounts of Nanofil were also seen in polymers containing only Nanofil and PVA. This result suggests that Nanofil weight percentages less than 5% could lead to additional conductivity gains. In the figure, the conductivity of PVA-KOH membranes with 5% Nanofil at different loadings of KOH are compared. The conductivity of these samples reached up to 0.095 S/cm at a 50 wt% KOH loading. Thus, the 0.1 S/cm goal for this project was reached. The membranes appeared to be mechanically strong such that they would make good battery separators.



*Conductivity of PVA-KOH membranes with 5 wt% Nanofil and varying weight percentages of KOH*

The PVA-KOH samples with 30% KOH were characterized by DSC and also XRD. In general, the melting temperature goes down as more additives are introduced. XRD data show that the addition of 5 wt% Nanofil decreases crystallinity in the polymer compared to either the 30% PVA-KOH polymer or the baseline PVA polymer. This decrease in crystallinity is most likely responsible for the increase in conductivity. This result builds off of the Year 1 results of the project showing that decreasing the crystallinity of the polymer is important to increasing the conductivity. More concentrations of clay near 5 wt% could be tested for further reduction in crystallinity in the future.

## **Self Assembly of Shape-Selective Catalyst Impregnated Membranes: Towards Direct Methanol Fuel Cells (DMFCs)**

*Simona E.Hunyadi Murph; H. C3lon-Mercado, E. Fox, R.D. Torres, S. Serkiz, L. Sexton, K. Heroux, J. Becnel, K. Herrington, M. Westbrook, S. Retterer (Oak Ridge National Laboratory), D. Hensley*

*The goal of this project is the development and evaluation of novel platinum (Pt) and Pt alloy nanostructures of various size, shape, surface structure, reaction site distribution (e.g. planar, edge, and corner), morphology and composition for DMFCs applications. We successfully self-assembled Pt nanocatalysts into Nafion membranes by either (a) an electrostatic approach or (b) an electric field approach. This resulted in more efficient utilization of precious metal in a way that can be further tailored to achieve desired catalytic activities while significantly reducing precious metal loading.*

Fuel cells have been studied extensively throughout the world as one of the most feasible next generation clean energy sources. Among the various types of fuel cells, the DMFC is the technology of choice for portable electronic devices. This is due to their high energy density by volume and weight, fast startup, immediate response to changes in the demand for power, and tolerance to shock. Moreover, a DMFC can produce continuous power by the direct conversion of the methanol fuel. This differs from a lithium battery that requires permanent recharging. The main advantages for the use of methanol as fuel are (i) its high energy density and liquid state at room temperature, (ii) its ease of storage and transport, and (iii) its relatively low cost.

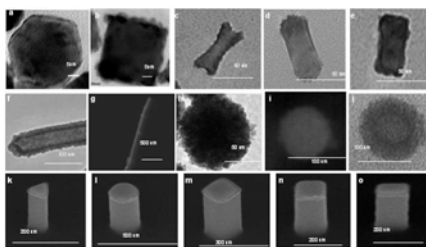
Catalysts serve two main functions in a DMFC. They facilitate the oxidation of methanol at the anode and the reduction of oxygen at the cathode. Currently platinum (Pt) and its alloys are the most effective catalysts for methanol electro-oxidation. From a practical point of view, Pt is one of the few active and stable noble metals that can withstand harsh environments. However, its high cost often hinders its use in large-scale commercial applications. As a result, one main goal of catalyst design for DMFCs is to reduce the precious metal loading by producing Pt catalysts with high surface area and low density. This increases catalytic performance and utilization efficiency. Decreasing particle size and creating nanomaterials with different morphologies are expected to boost the performance of the Pt catalyst and reduce the cost and overall weight of the FC. Further reduction in cost will result from efficient distribution of Pt catalysts at the three-phase interface region (catalyst/carbon/electrolyte) for an effective proton, electron and gas transport to and from the catalyst sites.

Large-scale commercialization of DMFCs has also been hindered by the inability of the electrolyte membrane to act as an effective methanol barrier. The methanol cross-over phenomenon leads not only to waste of fuel, but also causes heat generation that

decreases power generation capability. Another common problem for DMFCs has been the CO poisoning of Pt catalyst surfaces during the electro-oxidation process. This slows the kinetics of the anodic reactions and results in a significant loss in fuel cell efficiency.

In order to overcome these issues, our research strategy was to (a) *produce and characterize nano-sized platinum and platinum-based materials* with different morphologies and compositions in order to maximize catalytic activity on a mass basis and (b) *develop self assembled Pt modified Nafion membranes* to improve catalyst loading, its distribution and utilization, while reducing methanol permeability and the cost and overall weight of DMFCs.

We have developed and optimized a seed-mediated growth approach to make unique Pt and Pt-alloy (Pt-Au, Pt-Ag) nanoparticles of controllable aspect ratio (length/width), with tunable shapes, size, configurations (solid and hollow), porosity, composition and physico-chemical properties. All these reactions take place in air and water, and in principle, are amenable to scaling up. Au or Ag nanoparticles were used as “seeds” for subsequent platinum growth. Small changes in reaction conditions were used to control the final morphology of these nanoparticles. Additionally, ordered arrays of Pt and Pd nanoparticles with different geometries including spheres, diamonds, squares, triangles, and rectangles, supported on Si posts were fabricated via electron-beam lithography at ORNL.



*Electron micrographs of representative Pt, Pt-Au, and Pd nanoparticles with unique shapes.*

Structural information such as the size, shape, thickness, aspect ratio, porosity, separation, and topology of different nanocatalysts were examined by multiple characterization techniques. The effective surface charge was monitored via  $\xi$  potential measurements while the final composition and metal surface distribution on a nanomaterial's surface was also determined.

Among the samples tested, the rod shaped and solid sphere nanoparticles showed very promising results for both methanol oxidation and oxygen reduction. Pt-Au nanoparticles are especially attractive as they show resistance to methanol oxidation in the presence of oxygen. In addition Pt-Au composites are expected to improve the stability of cathode electrocatalysts as they decrease the interaction of the Pt catalyst with the carbon support by having an inert gold interlayer. This will result in the reduction of the catalytic

corrosion of carbon by the direct contact of Pt with carbon. The samples prepared at CNMS-ORNL are currently under investigation and will be reported on at a later date.

We successfully self-assembled Pt nanocatalysts into Nafion membrane by either (a) an electrostatic approach or (b) an electric field approach. Based on their properties (surface charge, size, shape), the nanoparticles showed different dispersion properties in the Nafion membranes. The ability to precisely self assemble Pt nanoparticles onto Nafion film allows for direct contact and maximum exposure of all active Pt catalysts sites. This resulted in efficient utilization of the Pt surface that can be further tailored to achieve desired catalytic activities while significantly reducing precious metal loading. This approach is expected to efficiently block the methanol crossover through the Nafion electrolyte membrane and enhance the performance of direct methanol fuel cells.

### **Advanced Batteries for Electric Energy Storage**

*Ming Au; Elise Fox, Hector Colon-Mercado*

*This project is developing advanced batteries with high capacity, low cost and enhanced safety for electric energy storage, particularly for electric and hybrid electric vehicles. The research activities focus on (1) rechargeable Li/air batteries – prove the concept of the rechargeability and (2) nanostructured Li-ion rechargeable batteries – develop free standing nanorods/nanowires for high capacity anodes.*

Li/air batteries present a new horizon for transformative electrical energy storage technologies for their revolutionary high energy density and low cost. However, two major obstacles prevent it from practice application: 1) the Li-air batteries are not rechargeable due to insoluble discharge products (lithium oxides) clogging cathodes; 2) their power density is very low limited by low solubility of oxygen in the polymer electrolyte. In the Li-ion battery category, Si is being investigated because of its large theoretic energy density as the anode, however, these batteries experience rapid capacity decays caused by large volume expansion. The proposed research targets these two challenges for the near term and ultimate solutions.

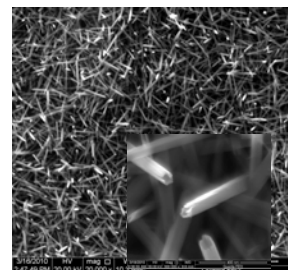
#### 1. Li/Air rechargeable batteries

To overcome the obstacles, three innovations were undertaken: (1) multilayered architecture of cathodes with pore size control to maximize the formation of tri-phase (solid-liquid-gas) area and host the precipitation of insoluble lithium oxides; (2) nanostructured dual functional catalysts that facilitates oxygen reduction and evolution both; (3) the hydrophobic non-aqueous electrolytes with sufficient solubility for oxygen and lithium oxides.

In the first year, the multilayered cathode architecture (hydrophobic layer-gas diffusion layer -active reaction layer), battery hardware and testing system were designed,

fabricated and set up. Two cathode fabrication processes, paste-rolling and buckypaper-filtration, have been parallel employed for comparison. Eight supported catalysts (MnPyr600, MnPyr900, MnSO<sub>4</sub>600, MnSO<sub>4</sub>900, Co-Urea-LS-800, LiPyr900, FePyr900, CoPyr900) and three un-supported catalyst (α-MnO<sub>2</sub> nanotubes, Fe<sub>2</sub>O<sub>3</sub> nanoparticles and Fe<sub>2</sub>O<sub>3</sub> nanospheres) were developed in house and tested using the rotating disk electrodes for their electrocatalytic activities. Unique square nanotubes of α-MnO<sub>2</sub> were developed with excellent electrocatalytic activity among the unsupported catalysts. It was found that the supported catalysts perform oxygen reduction better than unsupported. Within supported catalysts, the activity order was as follows: Mn and Fe > Li > Co.

Li/air batteries with and without catalysts were fabricated using two cathode fabrication processes and tested. The Li/Air battery without catalysts exhibited low initial discharge capacity (700mAh/g) and can not be recharged after discharged. The Li/Air battery with catalysts (α-MnO<sub>2</sub> nanotubes) demonstrated high initial discharge capacity (2500mAh/g) and rechargeable with average capacity of 600 mAh/g in 50 cycles. It proved that the catalysts play the role in reduction of lithium oxides. However, only the portion of lithium oxides able to access the catalysts can be reduced. The rest lithium oxides will be accumulated in the pores of the cathodes and eventually clog the pores resulting in oxygen deficiency and gradual decrease of capacity. This proved that (1) our Li/air batteries are rechargeable in limited cycles; (2) α-MnO<sub>2</sub> nanotubes are excellent catalyst for oxygen reduction and revolution. The comparison shows that the cathodes made by filtration process perform better than paste-rolling process attributing to precise architecture control and thinner layer.



*SEM image of α-MnO<sub>2</sub> square nanotubes*

Seven ionic liquids were acquired and evaluated for their ionic conductivities and the solubility for the lithium salts. Among them, 1-butyl-3-methyl-imidazolium TFSI has solubility for lithium salts with a good conductivity of  $3.38 \times 10^{-3}$  S/cm. The selected ionic liquids have used as electrolytes for Li/air batteries and being tested.

## 2. Nanostructured Li-ion rechargeable batteries

To sustain high capacity of Si anodes, the Si nanorods with gradient of Cu were synthesized and retained the capacity of 600 mAh/g in 100 cycles. The concept of the rechargeable Li/air batteries was proved by experiments. The multi-layer cathode architecture and two fabrication processes were developed and validated. The effective catalysts were synthesized using pyrolysis and hydrothermal processes both. Suitable ionic liquids were identified through conductivity screening. All project objectives for this first year have been exceeded. One utility patent has been filed, and two disclosures have been deemed patentable. In the second year, the project will focus on a cathode architecture that provides maximum tri-phase area and the novel electrolyte that offers sufficient solubility for lithium oxides and oxygen.

## **Thermodynamic evaluation of metallic waste forms for nuclear materials**

*Mark Williamson; Stephen Garrison, Lindsay Roy, Lindsay Baxter*

*This project explored a new method of evaluating metallic waste forms for waste generated from spent nuclear fuel reprocessing. These results support DOE environmental management mission areas and expand our capabilities in the field of nuclear fuel recycling and radioactive waste management. The knowledge gained through this work not only provides a fundamental understanding of metallic waste form alloys and their microstructures, but also improves our ability to reliably predict the chemical behavior of such materials in a variety of environments. Our protocol will enable researchers to cost-effectively evaluate the suitability of alloy compositions for geological disposal.*

The recycle strategy for commercial used nuclear fuel leads to metallic waste species that would be destined for placement in waste forms for repository disposal. Current efforts include immobilization of noble metal fission products by encapsulation, chemical transformation, and/or inclusion in a stable material. The IWMS Waste Treatment Baseline Study report suggested a metallic waste form alloy be used as a baseline for immobilization of undissolved solids, technetium, and noble/reduced metals from TRUEX raffinate produced during processing. An Fe-based alloy as a candidate alloy waste form was developed at SRNL that is capable of capturing several fission products not removed during electrometallurgical treatment of spent nuclear fuel. The Fe-based alloy is essentially an Fe-Zr-Mo alloy with four primary phases have been by XRD as:  $ZrFe_2$ ,  $MoFe_2$ ,  $\alpha$ -Fe, and a Rh-rich phase.

Re, a surrogate for Tc, is captured by the Fe-Mo phase, Ru and Pd are captured by the Fe-Zr phase, and none of the noble metal fission products show appreciable solubility in  $\alpha$ -Fe. The fourth phase, the Rh-rich phase, has only been found in small amounts and is only notable in its relatively high Pd concentration. Research in the field has led to significant advances in new waste forms but the program approach tends to be quasi-Edisonian. Experimentalists have not assessed the efficacy of using Re as a surrogate for Tc in engineering scale productions, cannot accurately predict if an alloy will contain one or more fission products, and have not optimized the loading scenarios to contain the maximum amount of radiological waste. Hence, there exists a need to develop tools capable of providing a cost-effective approach in determining if an alloy will be suitable for waste remediation processes.

Using the Fe-based alloy results as a basis, this project has successfully addressed this challenge by developing a protocol for screening the solubility of noble metal fission products in potential alloys using quantum chemical methods. The detailed research objectives include i) evaluating the value of Re as a surrogate atom in experiments; ii)

investigating the solubility of noble metal fission products in the microstructures found in waste form alloys; iii) predicting a concentration limit in the microstructure; and iv) predicting the phases that are likely to be present in the alloy. We accomplished three out of the four objectives, as outlined below.

Our protocol for predicting the solubility is based on using Density Functional Theory to calculate the substitution energies for the fission metal-substituted structures at several different atomic concentrations. We focused on low concentrations to prevent large structural deviations in the alloys. From the data, the results can be extrapolated to find the theoretical maximum substitution limit of each fission metal in the structure. To test the efficacy of our protocol, we looked at the solubility of the metal fission products as a function of atomic percent substitution in three of the phases in the Fe-Zr-Mo alloy; MoFe<sub>2</sub>,  $\alpha$ -Fe, and Rh. In the Fe-Zr phase, there are three possible structures that can form and a complete analysis was not possible in the timeframe of the project.

Our first objective was to evaluate the role of Re as a Tc surrogate in waste remediation efforts using the experimental results from the MoFe<sub>2</sub> and  $\alpha$ -Fe microstructures in the Fe-Zr-Mo alloys. Calculations predict that substituting a Tc or Re atom into the  $\alpha$ -Fe and MoFe<sub>2</sub> cells are calculated to be energetically favorable ( $E_{sub}$  is negative) at fairly high concentrations. However, Re is considerably more soluble in the phases than Tc, and we attribute the enhanced solubility to the larger radial extent of the Re  $d$  shell when bonding to the atoms. Of the two cells, both atoms prefer substituting into the Mo sites in MoFe<sub>2</sub>. These results are in sharp contrast to experiment which predicts that a substoichiometric amount of Fe is contained in an Fe-Mo-Re phase. Because the atomic sizes of Tc and Re are similar to Mo, we suggest that another phase is being formed to account for the disparity. Using a polynomial regression, the calculations predict that 21.6 (27.8) atomic % of Tc (Re) should incorporate into  $\alpha$ -Fe structure, and 38.7 (42.9) atomic % of Tc (Re) should incorporate into MoFe<sub>2</sub> structure. Hence, Re should be more soluble in the metal waste form alloys and any concentration limit should be seen as ~5% overestimate to the amount of incorporated Tc expected.

After establishing a method to calculate the substitution energy, we examined the solubility of other high yield fission products (Zr, Mo, Ru, Rh, Pd) in MoFe<sub>2</sub>,  $\alpha$ -Fe, and Rh phases of Fe-Zr-Mo alloy. The fission product atoms show a stronger preference for MoFe<sub>2</sub> over  $\alpha$ -Fe phase. The calculations predict that the early- to mid-transition metals easily substitute into the structures whereas the platinum metals Rh and Pd are not soluble. This trend can be rationalized on the basis that as you traverse along a row, the  $d$  orbitals become stabilized and the substituted atom will have less orbital mixing and covalent behavior with the other atoms. Technetium is predicted to be the most soluble atom in MoFe<sub>2</sub> and  $\alpha$ -Fe, followed by Ru. To explain Tc solubility, Mulliken population analysis shows an unusual electronic configuration of  $4d^65s^1$  for Tc. It appears that the extra Tc  $d$  electron is responsible for polarizing the  $d$  states at the Fermi level and stabilizing the electronic structure.

Perhaps most significantly, we validated experimental results that Rh should remain a metal in the alloy. Calculations also predict that the most soluble fission atom is Zr while the least soluble is Pd. Our results are not taking into account that the microstructure  $ZrFe_2$  is comparatively more stable than Zr point defects in the Rh structure and we do not expect Zr to incorporate into the Rh structure in experiment. Also we can only speculate that the reason for the high Pd concentration in the Rh metal is that the Zr-Fe microstructure reached the concentration limit of Pd and excess has been deposited alongside Rh since both crystallize in the same space group.

### **Sorption of CO<sub>2</sub> into Supported Ionogels for Advanced Carbon Sequestration Technologies**

*J. Gray; B. Garcia-Diaz, S. Sherman, K. Huang (Univ. of S. Carolina), and T. Adams*

*Ionogels are ionic liquids mixed with a gelation agent or polymeric support to alter their physical and chemical properties. Ionogels have been investigated as novel electrolytes for electrochemical applications such as batteries and other specialized electrochemical systems. This project tests the electrochemical characteristics of ionogel materials for the electrochemical conversion of CO<sub>2</sub> to hydrocarbon fuels such as syn-gas, methanol and ethanol. In a related effort, a cost analysis of several Mixed Electron and Carbonate Ion Conductor membrane processes used to concentrate CO<sub>2</sub> for sequestration or processing was conducted.*

The creation of conductive solid or gel electrolytes using ionic liquids, known as ionogels, is an emerging field for electrochemical systems where conductive solid state materials are needed for flexible applications. Little is known about how interactions between the gelation agent and ionic liquid affect the performance of the material in different applications. Analysis of these interactions is made more difficult by the variety of ionic liquids that can be synthesized and the mixtures with different gelation agents.

Some ionic liquids are well-known to have relatively high absorption rates for CO<sub>2</sub> which can be further enhanced by the addition of complexing agents such as monoethanol amine (MEA). Ionic liquids with amine moieties have even been synthesized to further enhance CO<sub>2</sub> uptake, but can have large changes in viscosity during the absorption and desorption of CO<sub>2</sub>. The formation of a rigid support structure with controlled morphology is a potential advantage for the electrochemical treatment of CO<sub>2</sub> in the ionic liquid. Solid supported ionic liquid membranes have been examined as CO<sub>2</sub> separation materials, but have been limited in terms of CO<sub>2</sub> throughput and thickness for separation surface area.

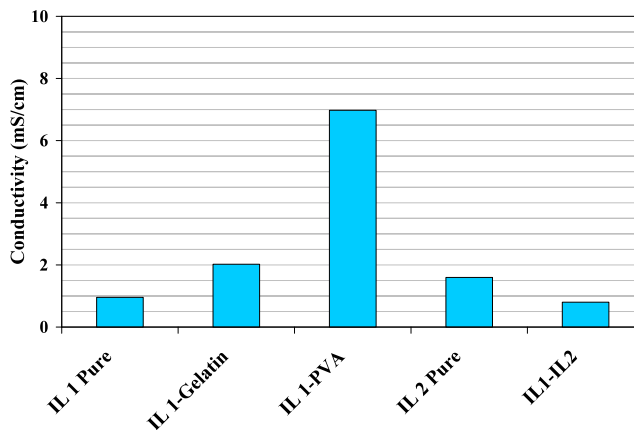
The work in this project examines the electrochemical conductivity of gelled ionic liquids with promising CO<sub>2</sub> uptake. The ionic liquids that were tested include 1-hexyl-3-methylimidazolium tris(pentafluoroethyl) trifluorophosphate ([HMIM][eFAP]) and 1-

butyl-3-methylimidazolium-2-(2-methoxyethoxy) ethylsulfate ([BMIM][MDEGSO<sub>4</sub>]). These ionic liquids are known to have favorable interactions with non-polar solvents and likely will have a high affinity for CO<sub>2</sub>. [HMIM][eFAP] has been shown to have higher CO<sub>2</sub> solubility than [BMIM][PF<sub>6</sub>] and [HMIM][Tf<sub>2</sub>N]. A similar ionic liquid, [HMIM][MDEGSO<sub>4</sub>], has a higher affinity for CO<sub>2</sub> than more common ionic liquids such as [BMIM][PF<sub>6</sub>] and [BMIM][BF<sub>4</sub>]. For convenience, [BMIM][MDEGSO<sub>4</sub>] and [HMIM][eFAP] are referred to as IL 1 and IL 2, respectively throughout the rest of this report.

Custom cells were designed and constructed in the machine and glass shops to facilitate forming the ionogels and testing the ionic liquids and gels for electrochemical characterization and performance. A significant amount of time was taken to find stable gelling combinations which formed a solid single phase. Many combinations of ionic liquid and gelling or polymeric supports tend to separate or become distended, and in some cases do not form soluble phases even at elevated temperature. Systems were selected which formed stable phases and which are known to absorb CO<sub>2</sub>.

These ionic liquids and the derivative supported gel and polymeric phases were then placed into a second set of custom built conductivity cells. These cells were designed to enable controlled 4-point conductivity measurements to be carried out on both liquid and solid phases.

These conductivities were measured using a potentiostat. In order to control the atmosphere as either ambient air or CO<sub>2</sub>, a cell was designed which enable the samples to be exposed to CO<sub>2</sub> at relatively mild overpressures of up to 14.7 psi (1 bar). This cell has four copper electrical contacts and a gas inlet and outlet to allow for controlled pressure measurements in a fully sealed environment.



*Conductivity of Ionic Liquids and ionogels for CO<sub>2</sub> absorption*

The conductivity for the pure ionic liquids and ionogels as measured by a four electrode impedance method are shown in the figure. The pure samples of IL 1 and IL 2 had conductivities of 0.83 mS/cm and 1.1 mS/cm, respectively. A 50-50 mixture of IL 1 and IL 2 had a conductivity value lower than the pure components at 0.57 mS/cm. These conductivity values are lower than for some more common ionic liquids due to lower polarity of the ions. However, ionogels synthesized with the ionic liquids increased the conductivity of the pure ionic liquid by 200% and 580% when using gelatin and PVA as gelling agents for IL 1.

The increase conductivity of the ionogels over the base ionic liquids is a promising development for being able to improve the electrochemical properties of ionic liquids that have good CO<sub>2</sub> absorption characteristics. The ionic liquids and ionogels that were synthesized are able to hold up to 20 mol% of CO<sub>2</sub> at 60 bar and should be very useful in being able to separate CO<sub>2</sub> from flue gas. The conductivity could also provide enough electrochemical performance to be an effective reaction medium for reduction of the CO<sub>2</sub> to biofuels. To create a viable process for capture of CO<sub>2</sub> and reaction, more research will be needed on finding optimum ionic liquid and gelling agent combinations to increase the conductivity while maintaining high CO<sub>2</sub> absorption.

An evaluation of the use of Mixed Electron and Carbonate Ion Conducting (MECC) membranes for electrochemical separation of CO<sub>2</sub> from flue gas streams was also conducted as part of this research effort. This innovative concept has been proposed by colleagues at the University of South Carolina, but little information is available about feasibility of these types of processes and their cost. Guidance from NETL on performance targets indicates that a 35% increase in the cost of electricity or lower is the acceptable price for removal of CO<sub>2</sub> from off streams from power plants for coal and natural gas. The analysis for different plant configurations using the MECC process showed that, in at least one configuration, ideally there was only an 11% increase in the price of electricity when CO<sub>2</sub> sequestration was added. However, when more realistic operating assumptions were used, the best option became a 17% increase in electricity cost. This 17% increase meets the DOE target of less than a 35% increase in electricity costs.

These two pieces of research scope are significant for the continued development of CO<sub>2</sub> separation and treatment research being pursued collaboratively by researchers at SRNL and USC. The laboratory results on the ionogels demonstrate one possible approach to simultaneously separate the CO<sub>2</sub> at point source locations while also delivering a possibility to convert the gas to a value-added product. A potential benefit of an electrochemical approach for CO<sub>2</sub> conversion is that in addition to temperature, pressure and choice of catalyst, the reaction progress and selectivity can also be controlled by manipulation of electrochemical potential. These preliminary data suggest that identified ionic liquid systems should be further pursued for study as electrochemical systems. The economic evaluation demonstrates that a technological concept under development by colleagues at USC is theoretically capable of meeting DOE targets.

## **Structure Property Relations in Mixed Ionic/Electronic Conductive Ceramics for Energy Conversion**

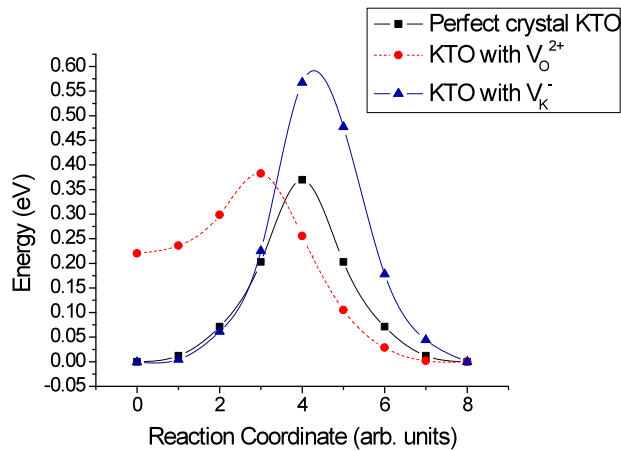
*K. S. Brinkman; R. Lascola, A. Mendez-Torres, D. Sholl (Georgia Tech)*

*This work focuses on structure property relations via microstructure modifications and first principle calculations aimed at understanding fundamental aspects of proton conduction in oxides. Metallic phase additions of Pd and Rh resulting in “dual phase” membranes, and alternative sintering techniques resulted in altered microstructures and defect distributions displaying enhanced conductivity at temperature and gas ambient conditions relevant to membrane separations, fuel cell and electrolysis cell operation. First principle investigations using Density Functional Theory examined the proton conduction mechanism under native point defect concentrations. It was found that the energy barrier to proton transfer was increased in intrinsically defective perovskites (metal and oxygen vacancy) compared to the transport in defect-free materials due to the coulomb attraction of oppositely charged defects highlighting the important role of point defects in these materials.*

Ion and electronic conductive ceramics are core components of ubiquitous energy conversion devices such as batteries, sensors, electrodes, fuel cells, catalysts, combustion devices and functional membranes. The charge carriers responsible for energy conversion are a result of both intrinsic (composition, nanostructure effects) and extrinsic (temperature, gas ambient partial pressure) effects. Traditional studies have focused greatly on compositional modifications, however it is now realized that processing induced defects via nanoscale material synthesis or alternative sintering methods need to be a key focus area for the design and fabrication of next generation energy conversion devices.

The present report described research activities focused on structure property relations via microstructure modifications resulting from i) first principles modeling of proton behavior in oxide materials, ii) alternative sintering technologies such as Spark Plasma Sintering (SPS), iii) material additions of 2<sup>nd</sup> phase metallic species Pd and Rh for enhanced conductivity. Following the discovery of proton conduction in ceramics of the form SrCeO<sub>3</sub> by Iwahara et al., dense ceramic membranes have received much attention due to their low cost and high efficiency in gas separation applications. In order to construct such a framework for understanding hydrogen in oxides, first-principles calculations were initiated, aimed at understanding fundamental aspects of proton conduction in a model KTaO<sub>3</sub> (KTO) with implication for other perovskite systems. Little is currently known about the mechanisms of proton transport in these materials, so initiating the rate limiting processes was an important first step towards rational engineering of materials compositions to enhance proton transport rates.

Density-functional theory was used to investigate the properties of KTO including quantum tunneling effects. Tunneling contributions are the dominant feature of  $H^+$  diffusion for  $T < 277$  K. We also elucidated the proton conduction mechanism under the native point defects. The magnitude of the activation energy is an important parameter that determines proton conduction in oxide materials. With respect to proton transport, coulomb charge repulsion was observed between the proton and the oxygen vacancy which is the most preferable native point defect. As shown in the figure, it was found that the energy barrier to transfer was increased compared to the transport in defect-free KTO due to the coulomb attraction between the potassium vacancy ( $V_{K^-}$ ) and positively charged proton  $H^+$ .



*DFT-calculated energies for proton moving along the minimum energy path in rate-limiting step for perfect crystal KTO and KTO including oxygen vacancy and potassium vacancy*

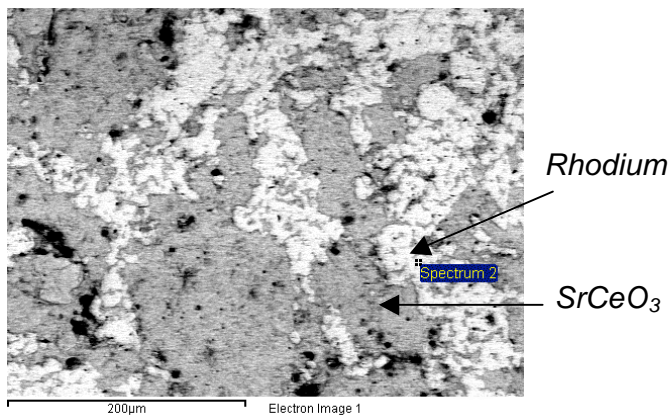
This electrostatic attraction between  $V_{K^-}$  and  $H^+$  could be a factor inhibiting the mobility of protons in KTO. It was also found that the migration energy barrier of an oxygen vacancy was 0.42 eV higher than the energy barrier for a proton to jump to a neighboring oxygen binding site. However, the energy barrier for oxygen vacancy migration can be lowered by 0.37 eV by insertion of a proton on a host oxygen lattice site resulting in hydroxyl group diffusion. This work outlined the important role of point defects in these materials systems.

Experimentally, point defects were examined using vibrational spectroscopy. Oxygen non-stoichiometry in doped  $CeO_2$  and  $SrCeO_3$  systems have been investigated using raman spectroscopy revealing bands near  $600\text{ cm}^{-1}$  that are associated with oxygen vacancies. The link between theoretical impact of lattice defects combined with experimental examination via spectroscopy provides an important insight into materials transport behavior. Future work in this area will involve the in-site examination of defect concentrations and transport behavior at temperatures and gas environments of relevance to membrane separations.

Bulk processed SrCeO<sub>3</sub> powders and chemically derived powders have undergone SPS trials at the vendor (Metal Processing Systems MPS). It was found that crystalline chemical derived and bulk oxide powders SPS sintered at 900°C (heating time 11 minutes, hold time 5 minutes) maintained the SrCeO<sub>3</sub> phase but achieved densities of only 66% (bulk oxide) and 78% (chemical) respectively. The grain size of chemical SPS was nominally 2 microns, slightly larger than the original particle size of 1 micron. Important differences in conductivity were observed between SPS and conventionally sintered samples. Chemically derived powders sintered by the SPS method displayed conductivity values near  $2 \times 10^{-4}$  S/cm, an order of magnitude above the conductivity of conventionally sintered samples  $3 \times 10^{-5}$  S/cm measured at 500°C in hydrogen atmospheres. Altered defect concentrations due to rapid heating in vacuum (SPS) as opposed to slow sintering in air are believed responsible for these differences.

In order to achieve smaller grain size in sintered materials, a trial of simultaneous “crystallization” and “sintering” was undertaken starting with 90 nm particle size amorphous SrCeO<sub>3</sub> powders. Four different trials were performed at temperatures from 800 to 1000°C, however only a trace SrCeO<sub>3</sub> phase formation was found. Later trials found sintering at 850°C for 10 minutes in vacuum produced increased quantities of SrCeO<sub>3</sub>, however CeO<sub>2</sub> was still the major crystalline phase present in the assemblage. Elevated temperature processing near 1200°C resulted in sample melting via the SPS process. Further work is required on the optimization of both chemical synthesis routes and SPS sintering parameters to obtain dense ceramic samples with nanometer grain size distributions.

Dual phase ceramic (SrCeO<sub>3</sub>) and metallic (Pd, Rh) membranes were fabricated in order to enhance the electronic conductivity and improve membrane separation efficiency. Metallic elements were chosen that would not oxidize under ceramic sintering conditions (1500°C air) and were added in a “percolating” ratio of 40 volume % metal in 60 volume % ceramic to ensure a network of metallic conduction through the membrane thickness. The figure below the microstructure of the dual phase membrane. X-ray diffraction analysis indicated no secondary phases were formed concomitant with metal additions. Metallic phase additions resulted in enhanced conductivity at elevated temperatures in hydrogen atmosphere as compared to single phase SrCeO<sub>3</sub> ceramics confirming the percolating nature of the developed membrane microstructure. Differences in Pd versus Rh additions were due to the difference in



*SEM Energy-dispersive X-ray spectroscopy (EDAX) elemental mapping indicating composite metal and oxide heterostructure*

hydrogen solubility ( $S \sim H/M$ ) and diffusivity ( $D \text{ cm}^2/\text{s}$ ) between the elements: Pd  
 $H/M=0.03$ ,  $D=10^{-4} \text{ cm}^2/\text{s}$  at  $400^\circ\text{C}$ , ( $Rh \ H/M < 0.03$ ,  $D=10^{-8} \text{ cm}^2/\text{s}$  at  $400^\circ\text{C}$ ).

### **The Impact of Climate Change on Future Energy Production in the Southeast US**

*David Werth; Lance O'Steen, A. J. Garret, Sebastian Aleman, Kuo-Fu Chen (University of Mississippi), Mustafa Altinakar*

*While there is general agreement that global climate change is occurring, it has become clear that we still are unable to predict its local impacts. Because of the importance of energy production in our economy, this project is focusing on developing methods to better assess what the impacts of climate change will be. This project has demonstrated the benefit of statistical downscaling and produced 21<sup>st</sup> century forecasts of climate with a much lower use of resources than had we run a mesoscale model for the decade. The application of this to power production represents a unique use of the science.*

The future energy profile of the American southeast may be dictated by climate change, as a shift to renewable energy sources that do not produce greenhouse gasses (GHGs) is generally seen as a good way to reduce their concentrations in the atmosphere. Hydropower is one such source, and is an attractive option if in the future GHG concentrations become unacceptably high. The future hydropower potential, while small for the southeast US however, is expected to be affected by climate change as temperatures rise and precipitation patterns change, and techniques developed here can be applied to other regions of the US where hydropower has the potential to be a more significant source of clean energy. Coal and nuclear power production (the latter being another non-GHG option) are also affected by climate change, as reduced flow and rising water temperatures make rivers poorer recipients of waste heat.

Future climate projections are therefore needed to predict possible future energy options. These cannot be provided by global climate models (GCMs), however, as GCMs are too coarse to resolve the small-scale climate changes that can affect energy production. Therefore, a process is needed to 'downscale' the GCM results to smaller scales. This data can then be fed into a surface hydrology model to help determine two things – the future hydropower potential of the southeast US, and the future ability of rivers and cooling ponds to remove excess heat from existing (or planned) plants, allowing us to determine their future ability to operate.

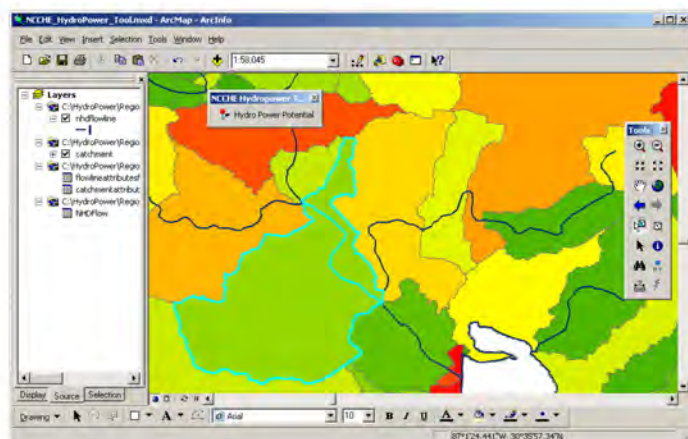
The first part of the project involves a statistical downscaling of data from a GCM. This comprises two parts. First, we must 'train' each selected method - use GCM and station data from the 20<sup>th</sup> century to establish the relationship between the two. Next, we apply the same relationship to GCM data from the 21<sup>st</sup> century, giving us the 'downscaled' data at the desired weather station.

Hydrologic models, using this climate data as input, are run to determine future flow rates. These flows are then used to determine the future hydropower potential. Simulations of the power plant cooling towers, lakes and river discharges with historical meteorological data are completed next. The same models will be run with projected meteorological conditions derived from the climate model simulations. The impact of more severe heat and reduced water availability on electrical generation will be quantified by comparing the two sets of simulations.

Three methods of downscaling GCM data (analog, scaling, and a neural network) have been developed and tested for Rome, Georgia using meteorological data from 1931 to the present. This location is near Plant Hammond, a 953MW coal-fired power plant operated and maintained by Georgia Power, and will be a station used to predict downscaled future precipitation and temperature for the Coosa River watershed which provides cooling water for Plant Hammond. When applied to the future GCM data, the existing relationships between the observed large-scale patterns (and, in the scaling method, historical GCM data) and the observed station data led to significant adjustments of the future GCM data, increasing the year-to-year variability of the temperature predictions and reducing the precipitation predictions. Taken together, the three forecasts represent an ensemble of forecasts for the 21<sup>st</sup> century, providing a range of possible climates for that time.

Watershed runoff models using the BASINS system were developed for each sub-basin upstream from Plant Hammond. The observed and the simulated flow duration for the Etowah watershed were in excellent agreement.

SRNL has received plant operating data from several power plants. A baseline year of 2001 has been established for the H.B. Robinson Plant. A simulation of the H. B. Robinson plant and its discharge canal predicts the cooling water discharge and intake temperatures within an RMSE of about 1.0 C relative to measured values. For future operations, this will require hydrological data from the BASINS model as input. SRNL has validated the mechanical draft and natural draft cooling tower models against data collected at SRS and with data from the open literature. This will make direct use of future meteorological data from the downscaling to predict future operations.



*Snapshot of the hydropower prediction tool*

New software has been developed by researchers at the University of Mississippi that calculates the potential hydropower of any region in the Southeast, given rainfall and temperature patterns (see figure above). The program must be calibrated using the BASINS explicit hydrological model at several stations using downscaled future climate data from those same stations as input, and these runs are now being conducted.

### **Fast Neutron Irradiation of Advanced Ceramics for Extreme Environments**

*E.N. Hoffman; D. Fisher, D. Diprete, M. Morgan, R. Sindelar, D. Vinson (Drexel University), M.W. Barsoum, D. Tallman*

*Limited information exists on the effects of radiation damage in ternary carbides. MAX phase carbides, such as  $Ti_3SiC_2$ , exhibit unique mechanical/physical properties due to their nano-laminate structure and bonding, making them promising candidates for GEN IV designs requiring very high temperature materials. This project established several new capabilities at SRNL. Two SRNL fast neutron irradiators have been developed using existing Cf-252 and Am-241/Be sources. A clean electropolisher for TEM sample preparation was assembled and utilized to prepare electron-transparent thin films of MAX phase materials. A bulk resistivity measuring capability was established, which measures resistivity of bulk samples without the need for permanent or semi-permanent attachment of measuring probes and allows for repeatable measurement that is not currently available in off-the-shelf products. Characterization was performed on the unirradiated or baseline properties of monolithic structures of several MAX materials.*

The demands made by Gen IV nuclear power plants on high temperature materials are severe. New materials will be needed to meet the service challenges of high temperature, neutron irradiation, and long lifetimes expected in Gen IV reactors. To date, SiC and SiC/SiC composites have received considerable attention as potential high temperature materials for neutron environments. SRNL has started exploring an exciting new material system as an alternative. A class of machinable, conductive, layered, ternary transition metal carbides and nitrides – the so-called MAX phases – are candidate materials for applications in neutron environments.

Research into the effects of fast neutron ( $E_n > 0.1$  MeV) irradiation at low levels of fast neutron exposure on the microstructural and physical/mechanical responses of MAX phase carbides have been initiated using existing Cf-252 and Am-241/Be sources as an SRNL fast neutron irradiators. This work provides the irradiation systems and capabilities for the characterization of the irradiation-damaged microstructures at the earliest stage of evolution, and of the resultant impact on the material properties. This work is complementary to high-flux irradiations ongoing at the MIT Reactor under an SRNL/Drexel University collaborative effort awarded by DOE-NE with post-irradiation characterization at SRNL, and at the Advanced Test Reactor under a user facility award. The research strategy involves irradiating and evaluating MAX phase carbides, with their inherent deformation-tolerance over a broad temperature-dose regime to explore their

response to displacement damage. A key investigation is the characterization of a neutron-damage microstructure on the kinetics of MAX phase kink-band formation, a unique damage mechanism rendering  $\text{Ti}_3\text{SiC}_2$  more resistant to fracture than traditional ceramics, such as SiC.

Three MAX phases,  $\text{Ti}_3\text{SiC}_2$ ,  $\text{Ti}_3\text{AlC}_2$ , and  $\text{Ti}_2\text{AlC}$ , were compared to SiC and Alloy 617, two leading candidates for the next generation nuclear power reactors, in an analysis of neutron activation for exposures to a neutron flux in a hypothetical fast reactor and a hypothetical thermal reactor. The simulated activation was performed using ORIGEN-S of the SCALE code system. ORIGEN-S computes time-dependent concentrations and source terms of radioisotopes, which are simultaneously generated or depleted through neutronic transmutation, fission, and radiological decay and in-growth. A single gram of each subject material was exposed to hypothetical fast reactor and thermal reactor neutron spectra for a period of 10, 30, and 60 years.

The activation products for each of the materials of interest were determined. These results show that the total activation of the MAX phases is similar to that of SiC and approximately three orders of magnitude less than Alloy 617 after 10 years of post-exposure decay, irrespective of the activation period in both the fast reactor and thermal reactor exposure. These results indicate that post-operation handling and disposal of the MAX and SiC materials would be improved; these materials would be disposed as Class C low level waste.

The contributions to activity for the initial discharge and the after a decay period of 10 years show that tritium and  $\text{C}^{14}$  are the primary radioisotopes in activated  $\text{Ti}_3\text{SiC}_2$ ,  $\text{Ti}_3\text{AlC}_2$ ,  $\text{Ti}_2\text{AlC}$  and SiC. The primary isotopes in Alloy 617 are  $\text{Co}^{60}$ ,  $\text{Fe}^{55}$ , and  $\text{Ni}^{63}$ . These primary radioisotope species are products of multiple step activation of the nominal constituents in the materials. That is, the common impurity species, such as N and O, do not significantly contribute to the activity.

Small samples of 5 MAX phases,  $\text{Ti}_3\text{SiC}_2$ ,  $\text{Ti}_3\text{AlC}_2$ ,  $\text{Ti}_2\text{AlC}$ ,  $\text{Ti}_2\text{AlN}$ , and  $\text{Ti}_2\text{SC}$  were exposed in the MIT pneumatic facility designated 2PH1 of the MIT Reactor to assess their activation in preparation for an irradiation campaign to investigate the materials' response to a moderate dose (up to 2 dpa), and moderate temperature (up to  $600^\circ\text{C}$ ) irradiation. The radioisotopes of the exposed samples were quantified by gamma spectrometry.

The specific activity of several isotopes generated by the exposure of the five MAX compositions shows very good agreement for the specific activity of  $\text{Sc}^{46}$ , an activation product of Ti. The disagreement between the results for Cr and Co indicates that there are some trace elements in the exposed samples that were not considered in the simulations. The iron results compare favorably, but the variability in measurement results indicate that the differences here may have been introduced by measurement error. Based upon these observations, it is expected that the models used in the current work provide reasonable accuracy in predicting the activation of the MAX and other materials.

Two separate fast neutron irradiators were developed by using two fast neutron sources; the Am-241/Be and the Cf-252 source. Samples of  $\text{Ti}_3\text{SiC}_2$  were exposed to the fast neutron flux from both sources. Resistivity samples of  $\text{Ti}_3\text{SiC}_2$  and CVD SiC were placed in a glass sample holder which positioned samples around the circumference of the source. Samples have been exposed to the neutron flux from the Am-241/Be source for 12 months. Mini-tensile, resistivity, and transmission electron microscopy samples of  $\text{Ti}_3\text{SiC}_2$  were placed in an aluminum sample holder with a tungsten lid attached by four aluminum rivets in the Cf-252 source. Samples were exposed to the neutron flux for 117 days.

Resistivity samples were tested using a portable resistivity jig connected to an ammeter and nanovoltmeters. TEM sample preparation was performed using an electropolishing sample preparation using a perchloric acid, ethanol solution. An electropolishing method was chosen over an ion milling method as it would result in the least amount of sample preparation damage. Ion milling can cause amorphization of the near-surface region in many ceramic materials.

No significant changes in the resistivity measurements of the samples exposed to Am-241/Be were detected.  $\text{Ti}_3\text{SiC}_2$  samples measured  $0.21 \mu\Omega\text{-m}$ , which agrees with values stated in literature. Measurements are yet to be performed on the sample exposed to the Cf-252 source.

To determine if a change in microstructure occurred as a result of the irradiation, optical, SEM and TEM samples were evaluated prior to exposure to the neutron flux. The grain size was found to be between 5-10 microns, typical of  $\text{Ti}_3\text{SiC}_2$ . X-ray diffraction was also performed on the samples, confirming the presence of  $\text{Ti}_3\text{SiC}_2$ , and secondary phases of TiC and  $\text{TiSi}_2$ . Samples post neutron exposure requires further evaluation.

No significant effect resulted from the Am-241/Be radiation flux. Activation occurred as a result of the 117 days in the Cf-252 flux. Additional testing will be performed to determine whether the resistivity changed as a result of the irradiation.

### **Organo-Boron Chemistries: Probing Variations in Lewis Acidity of Substituted Boroxines**

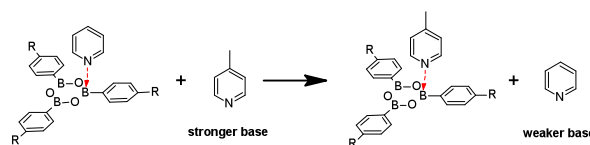
*Lucile C. Teague; Henry Ajo, William R. Kwochka (Western Carolina University), Tyler D. Jones, Terryol Wilson, Christine O. Bazinet and Heather Hawkin*

*Work continued on understanding the chemistry of boroxines, which are potentially applicable to a variety of SRNL programs.*

Trivalent boron compounds, such as boranes, boronates, and boroxines, are weak Lewis acids and readily form stable complexes with electron donating species which makes them excellent candidates for applications in molecular and environmental sensing and in “bottom-up” surface assembly processes. The work herein focused on understanding the reactivity of boroxines, which have gained recent attention for applications in gas storage

and sensing, battery technologies and non-linear optical materials. More specifically, this work was aimed at understanding the unique ligand binding chemistry of organo-boron materials, the influence of electron-withdrawing and/or electron-donating substituents on the specific bonding mechanisms, and their potential use as components for surface modification and “bottom-up” assembly of functional thin-films.

Our research has focused on the synthesis and subsequent analysis of conjugated organo-boron materials. Over 40 organo-boron molecules have been synthesized for NMR based solution-based exchange studies, fluorescence studies and surface attachment studies.



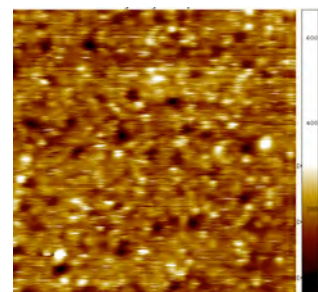
To further understand the influence of electron-withdrawing and/or electron-donating substituents on the specific complexation mechanisms specific mechanisms of organo-boron materials, a systematic displacement study was performed in which organo-boron-amine complexes were reacted with a variety of amines and monitored by NMR as we varied the electronic environment (R group) of the boron atoms. These experiments have helped us understand how to manipulate trivalent boron compounds for future applications in selective or “tunable” sensors. Fluorescence data reveal that the fluorescence response of these materials shifts both as the R-group is varied on the boroxine and upon complexation with various electron rich species.



*Fluorescence of uncomplexed (left) and complexed (right) boroxine*

Density functional theory methods were used to further understand how slight changes in chemical structure (variation in electronic environment of the borons) can affect complexation. Specifically, the bond dissociation energies of a variety of complexes were determined and compared with NMR data. We also compared calculated HOMO-LUMO energy gaps to the observed shifts in optical properties.

Several compounds synthesized for surface attachment have been deposited on the surface and subsequently analyzed via scanning tunneling microscopy (STM) methods. Surprisingly, molecular layers of boroxines were not able to be imaged on graphite surfaces, however, boroxines, boronates, and a variety of amine-complexed organo-boron materials were found to form monolayers on the Au(111) surface. Although molecular ordering was not observed in STM images of these films, XPS further confirmed molecular attachment to the surface.



*50 nm x 50 nm STM image of boroxine-amine complex on Au(111)*

Understanding the reactivity of these materials in solution and

on the surface has potential impacts in a variety of disciplines. Our work has shown that (1) these materials exhibit fluorescent behavior further showing their potential as fluorescence based sensors for electron-rich species such as amines and ions; (2) through exchange mechanisms, these sensors may be tunable to detect specific species; (3) these materials may be used as building blocks for the preparation of materials with tunable optical properties, and (4) these materials may be used for surface-bound sensors or as surface-modification layers.

The materials synthesized have been utilized to better understand the fundamental aspects of electrical interactions at the atomic level, which is crucial for the development of materials and methods needed for next generation environmental sensors, energy collection/storage devices, and environmental collection and detection materials.

### **Formation of Actinide Solid-Solution Oxides by Co-Precipitation of Actinide Oxalates**

*G. F. Kessinger; E. A. Kyser III, P. M. Almond, M. G. Bronikowski*

*Our results demonstrate the formation of U-Np-Pu solid solution oxalates by co-precipitation; furthermore, the results show that conversion of these oxalates to oxides is feasible. These results are important because:*

- *The solid solution oxalate is a pathway for the formation of MAMOX fuels that does not involve separation of Pu from the other actinides during used fuel processing.*
- *Utilization of recycled actinides in MAMOX fuels would reduce the volume of waste dispositioned to a waste repository.*
- *The homogeneity of solid solution oxide fuels should result in fuel materials with more predictable physical and chemical behavior.*

A recently proposed approach to mixed-oxide fuels (MOX), MAMOX (Minor Actinide MOX-fuels containing oxides of U, Np, Pu, and Am), uses actinides recovered during used fuel processing. This approach, as presently envisioned, utilizes physical mixtures of actinide oxides for fuel fabrication. We investigated the formation of mixed actinide oxalate solid solutions and the conversion of those solid solution oxalates to solid solution oxides. Using recycled actinides for fuel production results in reduced waste volumes. In addition, co-precipitation of actinides leads to reduced separation steps during actinide recovery and reduced proliferation concerns related to Pu separation (as compared to processes requiring separated Pu, Np, and Am). Lastly, the solid solution route is expected to produce more homogeneous oxides than the physical mixtures, resulting in fuels that have more predictable physical and chemical behavior.

Our approach to this problem followed an “applied science” pathway. Actinide metals in nitric acid media were selected as the starting point for our precipitations because most commercial used fuel processing flowsheets utilize nitric acid as the digestion solvent.

X-ray powder diffraction (XRD) was used to identify the crystalline phases formed during precipitation and calcination experiments. Because the co-precipitation of actinide oxalates is poorly understood, more time was spent investigating that phenomena than the better understood oxalate to oxide conversion process.

Baseline experiments were performed to determine how the actinide species present in nitric acid media would precipitate. As expected, these experiments resulted in the formation a U(VI) oxalate that was not present in the same phase as the Np and Pu oxalates. It is interesting to note, however, that the crystalline structures of the two phases present suggest that  $\text{Np}(\text{C}_2\text{O}_4)_2$  and  $\text{Pu}(\text{C}_2\text{O}_4)_2$  precipitated in the structure expected for  $\text{U}(\text{C}_2\text{O}_4)_2$ . Precipitation of mixtures of 1:1 molar ratios of Pu(IV):Np(IV) resulted in a single phase with the  $\text{Np}(\text{C}_2\text{O}_4)_2$  structure, demonstrating that a binary solid solution oxalate of Np and Pu could be produced. Calcination of these solids result in a single phase oxide, with reflections indicative of a solid solution oxide, demonstrating that it was possible to both precipitate Np and Pu as a solid solution oxalate and form Np-Pu solid solution oxides via the oxalate pathway.

Precipitation of U(IV) with quadrivalent Np and Pu requires that U in the nitric acid media be reduced from U(VI) to U(IV). Reducing uranyl to U(IV) in nitric acid media, and subsequently stabilizing the U(IV) species, is difficult since the nitrate ion readily oxidizes U(IV) under these conditions. A two-step approach was developed. First, a nitrite scavenger, hydrazine, was added the U-bearing solution. Second, the chemical reductant was added to the solution. Two metallic chemical reductants, U and Fe, were selected for study. The results of these investigations suggest that Fe was very effective for reduction of U(VI) to U(IV).

The first co-precipitation experiments involved U and Pu; later experiments involved U, Np, and Pu. The solids resulting from the U-Pu experiments were subjected to XRD analysis; reflections corresponding to the phases  $\text{U}(\text{C}_2\text{O}_4)_2$ ,  $\text{UO}_2\text{C}_2\text{O}_4$ , and  $\text{Pu}_2(\text{C}_2\text{O}_4)_3$  were identified in the solids from each of these experiments. These results suggest that it is possible to precipitate quadrivalent U and Pu in a single phase; however, it should be noted that the there were side reactions between U(IV) and Pu(IV) that resulted in the formation of some Pu(III) and U(VI), which also precipitated. There were also indications of formation of another unidentified phase, perhaps an oxalate solid solution containing an actinyl oxalate.

X-ray diffraction analysis of the solids from the U-Np-Pu precipitation experiments generally showed the presence of two phases,  $\text{U}(\text{C}_2\text{O}_4)_2$  (major phase) and  $\text{UO}_2\text{C}_2\text{O}_4$  (minor phase). These results demonstrate that it is possible to precipitate quadrivalent U, Np, and Pu into a single oxalate solution phase with the structure of the  $\text{U}(\text{C}_2\text{O}_4)_2$  phase.

## **Nanoscale Boron Based Neutron Detectors**

*Steven Serkiz; Lindsay Sexton, and Joe Cordaro*

*We have demonstrated the feasibility of using nanoscale boron-based materials as neutron detectors. If development continues to be positive, these could alleviate impacts of the current shortage of helium-3 by providing a viable alternative to helium-based proportional counters.*

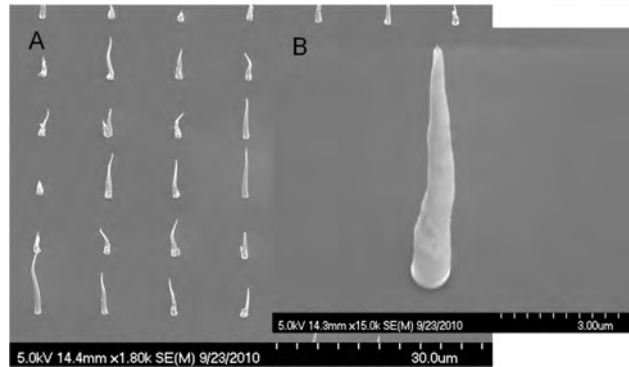
The helium-3 ( $^3\text{He}$ ) gas proportional counter (PC) is the “gold standard” for neutron detectors. Since 9-11, the Department of Homeland Security has been attempting to deploy neutron detectors at hundreds of domestic and international ports throughout the world to provide detection of special nuclear material. The demand for  $^3\text{He}$  as a fill gas in neutron detectors has, therefore, increased greatly and the available supply of  $^3\text{He}$  is projected to fall significantly short of demand in the near future.

This work seeks to develop a neutron detector that can achieve detection efficiencies similar to the  $^3\text{He}$  PC without the use of  $^3\text{He}$ , and, thereby, alleviate the  $^3\text{He}$  shortage. As an alternative to the  $^3\text{He}$  PC detector, we proposed to develop and test a working prototype of a boron-based nanoscale PC that would eliminate the need for  $^3\text{He}$  in neutron detection. This approach takes advantage of the large neutron capture cross section of  $^{10}\text{B}$ , the inherently high electrical field associated with nanoscale anodes in a PC, and the close proximity of the  $^{10}\text{B}$  to the anode (point of charge collection for the secondary ionizing radiation source). Two possible designs for this approach are; boron incorporated directly into nanoscale anode itself; and/or incorporating the boron into the substrate of the anode array or the cathode counter-electrode.

The overall approach of the proposed work is broken into two objectives: (1) produce nano-scale anode arrays that contain boron as an alternative to  $^3\text{He}$  filled neutron detectors, and (2) test these nano-scale anode arrays at SRNL in a gas proportional counter filled with a standard fill gas (e.g., P-10) exposed to a neutron source of known characteristics. The first objective can be further broken down into 4 tasks: (1) fabricate nano-scale arrays with controlled pitch, (2) test the electrical properties of nanoscale arrays, (3) test proportional response of arrays with a gamma source, and (4) doping of arrays with boron.

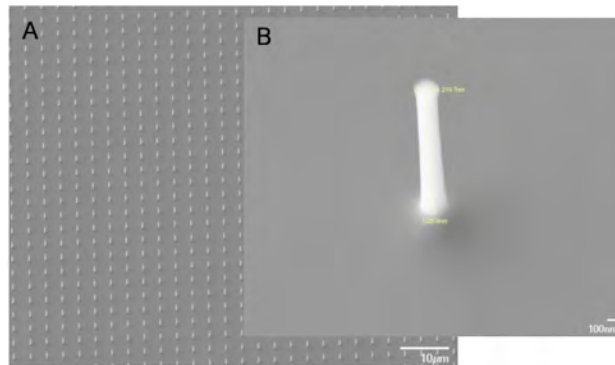
Nanoscale arrays with controlled pitch (i.e., nano-anode spacing) and anode size were fabricated at the Center for Nanophase and Materials Science (CNMS) located at Oak Ridge National Laboratory (ORNL). Arrays of both vertically aligned carbon nanofibers (VACNFs) and silicon posts were produced on p-type  $\langle 100 \rangle$  boron (B)-doped silicon wafer substrates. This B-doping provides both a conductive substrate and an array material already doped with the boron for neutron detection studies (Task 4). Use of pre-doped Si wafers may eliminate the need to further dope the nanostructures or Si substrate, however, further testing will be necessary to determine if this is the case.

The arrays produced consisted of nanostructures that were ~100 and 200 nm in diameter with pitches of 1, 2, 3, 5 or 10 microns. The arrays were defined using electron beam lithography to deposit 100 and 200 nm diameter metal catalysts (VACNFs) or masks (Si posts) with the previously mentioned spacing. The VACNF arrays were subsequently grown at the metal catalyst locations using plasma enhanced chemical vapor deposition (PE-CVD), while the silicon posts were etched using reactive ion etching (RIE). In the case of PE-CVD, the metal deposited (i.e., Ni) during the electron beam lithography process acts as a catalytic site from where the carbon fibers grow up from the surface (Figure 1).



(A) SEM image of a VACNF array with a 10  $\mu$  pitch. (B) SEM image of a single VACNF

In contrast, in RIE the metal (i.e., Cr) acts as a mask as reactive gases are introduced to etch away the exposed Si surface, leaving behind Si pillars where the metal was deposited (see below).

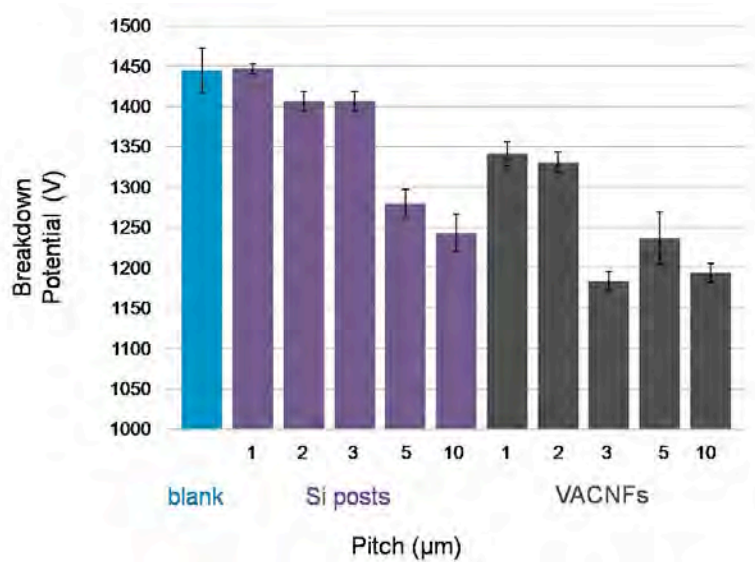


(A) SEM image of a Si post array with a 3  $\mu$  pitch. (B) SEM image of a single Si post

A 2.75" diameter six-way stainless steel vacuum chamber was setup to test the electrical properties of the nanostructured arrays as well as to perform proportional counting experiments. Inside the chamber, two parallel electrodes (Si wafer with the nanostructured array as the anode and an aluminum plate as the cathode) were separated by a spacer. The electrodes were connected through one arm of the chamber to a

preamplifier, which was connected to a high voltage source, a multichannel analyzer and an oscilloscope to measure pulses.

The electrical properties of the nanostructured arrays was tested by measuring the high voltage breakdown (an indirect measure of electrical field strength) between the array and aluminum cathode plate in parallel plate geometry. Breakdown studies were conducted in He at atmospheric pressure with a plate spacing of 0.5 cm. Under these conditions, the blank B-doped Si wafer gave a breakdown potential of  $1450 \pm 30$  V. The electric field strength associated with the nanostructures should be much higher than that of the blank Si wafer at the same potential and would be calculated to result in a lowered breakdown potential. The arrays of Si posts with pitches of 1, 2, 3, 5, and 10 microns gave breakdown potentials of  $1450 \pm 10$ ,  $1410 \pm 10$ ,  $1410 \pm 10$ ,  $1280 \pm 20$ , and  $1240 \pm 20$  V, respectively. The arrays of VACNFs with pitches of 1, 2, 3, 5, and 10 microns gave breakdown potentials of  $1340 \pm 20$ ,  $1330 \pm 10$ ,  $1180 \pm 10$ ,  $1240 \pm 30$ , and  $1190 \pm 10$  V, respectively. These data are plotted below, showing a lowering in breakdown potential with the Si post arrays having pitches greater than 5 microns, while all of the VACNF arrays show a reduced breakdown potential. The greatest decrease in high voltage breakdown was observed with the 3, 5, and 10 micron pitches, a result that is consistent with electric field modeling that predicted a spacing of at least 2.5 times the length of the nanostructure was required to preserve the electric field strength associated with the nanostructure.



*Breakdown potential in He at 1 atm and 0.5 cm electrode spacing for blank boron-doped Si wafers (blue), boron-doped Si wafers with nano-scale Si posts (purple), and boron-doped Si wafers with VACNFs (gray)*

We have begun testing the proportional response of the VACNFs and Si post nanoscale arrays arranged in parallel plate geometry with a 10 mCi Am-241 gamma source. The nanoscale arrays with 5 and 10 micron pitches exhibited an increased count rate

compared to a blank boron doped Si wafer at the same applied potential. An increase in count rate was observed with the 100 nm diameter VACNFs and Si posts compared to 200 nm diameter VACNFs arrays. We are in the process of optimizing operating conditions (i.e., gain settings, count times, etc.) to define the proportional operating region. Preliminary results show that 10 micron pitch arrays of both Si posts and the VACNFs reach the proportional region at around 40 V applied bias.

### **Evaluation of the long-term effectiveness of enhanced soil remediation with mixed amendments using geochemical parameters under field conditions**

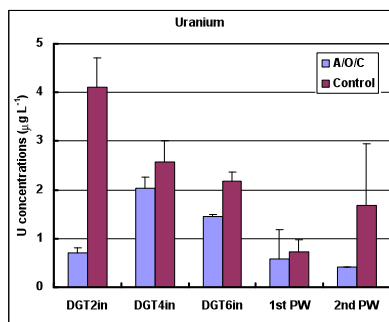
*Anna S. Knox and Kenneth L. Dixon*

*The evaluation of amendment mixtures provided a basis for the quantitative assessment of the long-term performance of the remediation technologies under field conditions. This technology should help to restore and sustain the environment on DOE, DoD, and commercial sites by reducing or eliminating the mobile pool of available contaminants in soils and providing a rational basis for long-term environmental management.*

The key question to be addressed by this project was the long-term performance under field conditions of amendment mixtures and their overall benefits in remediation of contaminated soils/sediments. The project included two major tasks: 1) evaluation of amendment mixtures for metal remediation under field conditions and 2) predicting the release of metals over time from remediated soil under field conditions.

The research was conducted in soil columns installed at a field site near Tim's Branch. The results have provided a basis for the quantitative assessment of the long-term performance of in-situ remediation with amendments under field conditions. Enhanced remediation with amendment mixtures containing e.g., apatite, organoclay, and chitosan (AOC) is more effective at sequestering metals than apatite (A) alone. Metal contaminants in treated soils and its mobility/bioavailability was determined by the comparatively new technology of diffusive gradient in thin films (DGT) as well as by standard methods for measuring the labile fraction of metals in contaminated soils. Metal contaminants occur in various physiochemical forms in the soil, some of which are tightly bound to the soil matrix and others of which are more labile. These labile fractions readily pass into solution where they are susceptible to uptake by plants and leaching into groundwater. Accurately distinguishing between metals in the solution and solid phases and understanding the exchange between these compartments is critical for estimating metal mobilization to groundwater and metal bioavailability, the latter of which determines the likelihood of successful remediation. The new technology of diffusive gradient in thin films (DGT) has the potential to provide this information. DGT was used in this project for measuring labile fractions of various metals in untreated soils and in contaminated soils treated with several amendment mixtures. The results showed the ability of DGT technology to accurately assess the mobility of metal contaminants in

unremediated and remediated soils (see below). Therefore, this technology can help to develop more accurate and cost-effective contaminant remediation strategies.



Mobile pool of U determined by the DGT method and measurements of metal concentrations in pore water; mixture of amendments (A- apatite, O- organoclay, C- chitosan)

### Advanced Gas Sensors Using SERS-Activated Waveguides

R.J. Lascola; C.S. McWhorter, S. Hunyadi Murph, B. Peters

*The goal of this project is the development and testing of a functionalized capillary that will provide detection of low-concentration gas-phase analytes through surface-enhanced Raman spectroscopy (SERS). Measurement inside a waveguide allows interrogation of a large surface area, potentially overcoming the short distance dependence of the SERS effect. Although we have not yet optimized the coating parameters, we have established the procedures and capabilities to address the basic components of capillary design – coating of the interior surface with an underlayer of metal to provide the waveguiding effect, attachment of the nanoparticles to the underlayer to add the SERS-generating element, characterization of the capillaries with high magnification techniques, and measurement of the Raman signal generated within the capillaries. The second year of this project will see the achievement of these goals along with the construction of a flow cell capillary holder.*

One of the axioms of the field of analytical chemistry is that there is no universal technique that is ideal for all analytes. There is a balance of strengths and weaknesses for each technique that must be considered when solving an analysis problem. The chemical composition, physical form, and accessibility of the material, as well as the presence of by-products and the sensitivity and ease of use of the method, are all factors. Accordingly, research and development in the field addresses a method's shortcomings, so that the method's advantages can be realized on a wider selection of samples.

This approach is expressed in our research to improve the sensitivity of Raman spectroscopy for gases. Raman spectroscopy is an optical technique in which light of a single color, as characteristically generated by a laser, is directed onto a sample. The molecules in the sample will scatter the light, with a small fraction of that light occurring

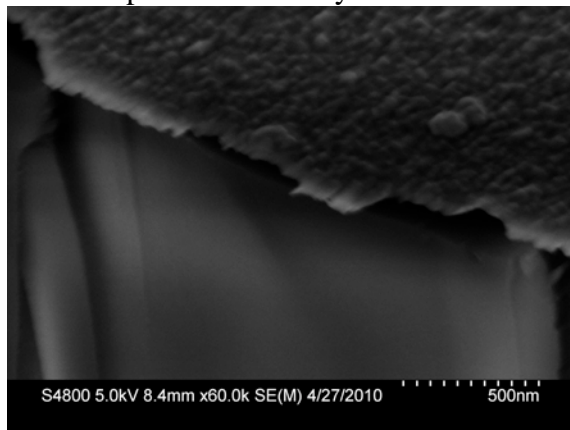
at different colors than the incident color. Both the identity and intensity of these new colors provide information that allows chemical identification and quantitation of the material. The advantages of Raman spectroscopy include the ability to detect certain types of molecules that are not detectable with other optical techniques, and the use of light in the visible region of the spectrum, which is easier to generate, manipulate, and detect. The disadvantage of the technique is that the fraction of Raman scattered light is exceptionally small, and thus the technique is relatively insensitive to those molecules which it can uniquely detect. This is especially problematic for gaseous samples, which are far less dense than solids or liquids.

Our method for improving the sensitivity of the technique combines two approaches. One is the use of a waveguide, or reflective tube, to expose more of the sample to the exciting light. The other is the modification of the interior of the waveguide with nanoparticles to increase the intensity of the Raman scattering (surface-enhanced Raman scattering, or SERS). Each of these techniques has been tried independently but they have not been combined, primarily due to the difficulty of preparing the SERS surface inside the narrow capillary. The goals of this project are: development of the surface modification, including the attachment chemistry; optimization of the Raman enhancements; and, ultimately, development of a prototype flow cell incorporating the waveguide. We anticipate that the combination of the two strategies could result in sensitivity enhancements on the order of 200-fold. If realized, this improvement would allow detection limits of Raman spectroscopy for gases in the low part per million level, with applications to weapons monitoring, process analysis, and field analysis of trace vapors.

We are using a commercially available Raman imaging probe to focus the laser light into the capillary. The Raman signal is collected in the backscattering mode, i.e. at 180 degrees. This arrangement simplifies setup because the optical design of the probe ensures that the field of view of the collection optics overlaps with the excitation volume. The capillary is held in a spring-loaded chuck mounted on a four-dimensional stage (3 linear adjustments plus rotation). This arrangement allows reproducible positioning and adjustment of the capillary.

The most effective SERS surfaces are based on either Au or Ag nanoparticles. We have chosen to work with a gold-based system, in which a thin layer of bulk gold is bonded to the interior of the capillary, followed by a layer of self-assembled nanoparticles. This approach is favored for several reasons. Gold particles and surfaces are more stable than silver. They better resist chemical attack and oxidation, and are more likely to retain their optical properties with repeated use. The underlying gold layer, made sufficiently thick, will convert the capillary into a waveguide. The chemistry of the attachment of the gold particles to a gold surface, through thiol linkages, is well understood.

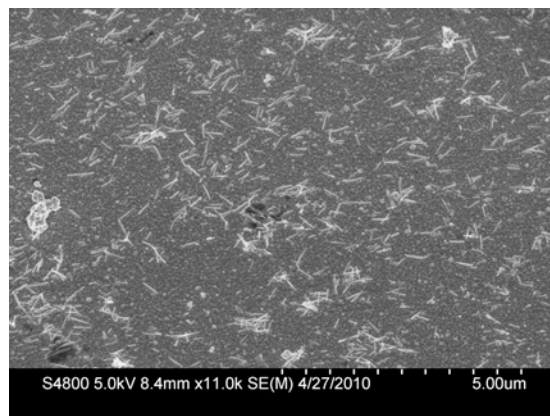
With respect to nanoparticle attachment, we are adapting solution-based techniques based on flat surfaces or large-diameter tubes for the smaller scale of a capillary. Initial work with a flowing solution of a lesser gold concentration produced thin layers on the order of 50-100 nm, as confirmed by scanning electron micrographs. There appears to be continuous coverage on the interior of the capillary, based both on visual inspection and on the SEM surface appearance. However, testing in the laboratory showed light leakage through the capillary walls. Subsequent work with more passes of a higher metal concentration solution resulted in a plugged capillary containing what is presumed to be gold salt. We have re-examined the coating chemistry and determined a new recipe that will provide better layer characteristics.



*SEM image of cross-section of (a) Au layer and (b) glass capillary*

Despite the light leakage, we observed Raman spectra of atmospheric  $N_2$  and  $O_2$  at 30% greater sensitivity compared to measurements in free space. This result gives us confidence that we will be able to generate greater Raman signals once the coating properties are optimized.

TEM images of high-aspect nanorods created at SRNL and attached to the thin gold surface inside a capillary are shown below. The nanorods shown have an aspect ratio of approximately 12:1 (~300 nm x 25 nm). These rods have an optical resonance associated with the shorter dimension that matches the 532 nm excitation wavelength of our system. The images shown here are for a dilute nanorod solution, resulting in incomplete surface coverage and minimal self-assembly. Optimization of this parameter is still required. These images were obtained from a fragmented capillary, and thus no Raman spectra were attempted for these samples.



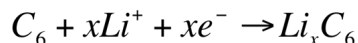
*Dilute nanorod deposition inside the capillary*

## Nano-Composite Hybrid Lithium-Ion Battery

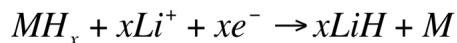
*H. R. Colón-Mercado; J. A. Teprovich, L. C. Teague, R. Zidan, J. P. Ganesan (University of South Carolina), B. N. Popov*

*During the project we were able to prepare, characterize and test graphite based batteries. The concept of using metal hydrides as battery anode electrodes was successfully proven. Based on the successful results using SRNL's novel nanocomposite materials for electrodes, more work will be done to optimize this new battery system.*

High energy density and safety are the most important requirements of commercial lithium-ion batteries when used to power portable electronic devices and vehicles. Generally, the more energy stored, the more hazardous and unstable the energy storage system is. In Li-ion batteries, one of the most hazardous events is the self-heating of a lithium-ion cell followed by a thermal runaway. In order to increase the specific energy of a battery, previous research has primarily focused on improving the performance of the anode. Li intercalation of anode materials such as graphitic carbon are often used rather than lithium metal to increase battery safety since intercalated materials are less chemically reactive than pure lithium. However, the specific energy of intercalated electrodes is an order of magnitude lower. In a typical Li-ion battery the anode electrode reaction consist of lithium ions intercalating in the graphitic carbon (charging step) as shown in the following reaction:



while the reverse will happen during the discharge step. The intercalation reaction occurs at a standard reduction potential of approximately -2.8 V. Pure metals are being studied as intercalation negative electrodes as they can provide specific capacities close to pure lithium; however these electrodes are subject to large volume changes following lithium insertion. This results in poor reversibility due to cracking and delamination of the electrode. This work addresses the issues at the negative electrode with a new set of nano-composite anode materials developed under the Basic Energy Science (BES) research program for hydrogen storage at SRNL. The new electrodes have similar or in some cases higher theoretical specific capacities than pure lithium metal, while being less chemically reactive, which increases the capacity without being hazardous. The use of metal hydrides as electrodes for Li-ion batteries has been demonstrated. When using metal hydrides as anode electrodes the following reaction takes place:

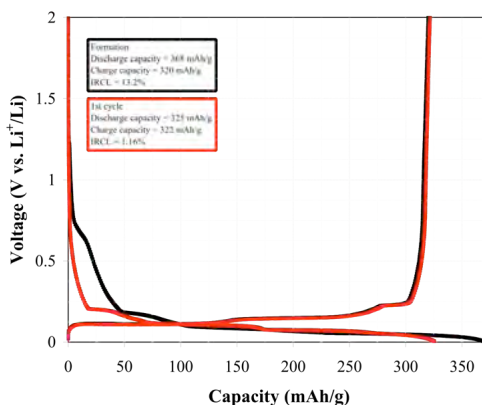


The work reported includes the initial results from the most promising new hydrogen storage materials prepared at SRNL in a Li-ion battery system.

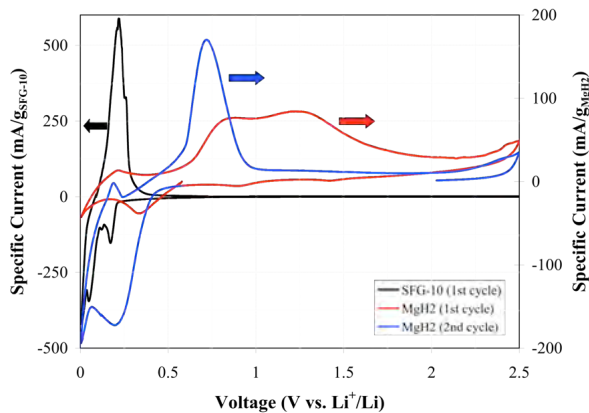
The first task of the work was to prepare a commercial Li-ion half cell with performance comparable to commercial performance. The use of metal hydrides such as  $\text{MgH}_2$  (2,037 Ah/kg) in lithium ion batteries has the potential at least doubling the capacity of commercial  $\text{LiC}_6\text{-Graphite}$  (372 Ah/kg) while providing appealing standard reduction potentials for anode applications. Figure 1 shows the topography of the electrode cast at SRNL compared to the commercially cast electrode.

The formation cycle of a half cell prepared at SRNL with commercial battery grade carbon SFG-10 (TIMCAL) is shown in the figure. As can be observed from the plot, we are able to reproducibly obtain during the formation cycle, capacities and IRCL (irreversible capacity loss) values comparable to those in the literature.

*Galvanostatic charge-discharge curves of SFG-10 with 10 wt% PVDF in 1 M  $\text{LiPF}_6$  EC-DMC based electrolyte*



Once the procedure to prepare batteries with commercial materials has been optimized, experiments to test the feasibility of SRNL's new materials were tested. Cyclic voltammograms of the prepared electrodes are shown in this figure. As we can see from the commercial anode, four main cathodic peaks (negative peaks) are observed. These peaks are related to the lithium intercalation in the graphite structure. In the case of the  $\text{MgH}_2$  anodes, the behavior changes from the first cycle to the second cycle. After the first cycle, the reactions remain the same. During the second cycle, we observe two main peaks. We speculate the low potential peak to be related to the intercalation of Li on the  $\text{MgH}_2$  matrix, while the peak at a higher potential to be related to the combination of the Li with the hydride (reaction potential of -2.51 V vs. Standard Hydrogen Electrode). Our nanocomposite materials were also made into electrodes and characterized by cyclic voltammetry. The CV results for our nanocomposite electrodes were very similar to the  $\text{MgH}_2$  electrode results and indicate that our nanocomposite materials can also reversibly form hydrides during the charge/discharge cycle of the battery through the intercalation/deintercalation of Li in our material.



*Cyclic voltammogram of SFG-10 with 10 wt% PVDF and  $\text{MgH}_2$  in 1 M  $\text{LiPF}_6$  EC-DMC based electrolyte at 0.05 mV/s*